MICROSTRUCTURAL ANALYSIS AND MODELING OF FLUE GAS DESULFURIZATION WASTEWATER SEQUESTERED IN THE ALKALI-ACTIVATED FLY ASH MATRIX

by

Morteza Ghaempanah Tajabadi

A dissertation submitted to the faculty of
The University of North Carolina at Charlotte
in partial fulfillment of the requirements
for the degree of Doctor of Philosophy in
Infrastructure and Environmental Systems

Charlotte

2019

Approved by:

_____

Dr. Jy Wu

_____

Dr. William Langley

_____

Dr. John Diemer

_____

Dr. Churlzu Lim

_____

Dr. Haitao Zhang

ABSTRACT

MORTEZA GHAEMPANAH TAJABADI. Microstructural Analysis and modeling of Flue Gas Desulfurization Wastewater Sequestered in the Alkali-Activated Fly Ash Matrix. (Under the direction of DR. JY WU)

Geopolymers can be categorized as synthetic zeolitic monoliths. The amorphous structure of this material is developed by dissolution of an aluminate and silicate-rich source, like fly ash, in a highly alkaline solution and then interlinking and crosslinking of Al and Si structures. These processes provide geopolymers with low permeability and resilience to physical and chemical attacks. The low permeability of geopolymers makes them a good candidate for solid waste immobilization. A host of research projects are dedicated to the immobilization of municipal waste incineration residue, carbon electric arc furnace residues and metal anions. However, the primary trials to immobilize flue gas desulfurization wastewater (FGD) have led into the disintegration of the geopolymer matrix. It is hypothesized that precipitates and crystals formed with anions (Cl^-, CO_3^{2-}, $C_2O_4^{2-}$ and PO_4^{3-}) and halides (Cl and Br) and gel components interrupt the formation of aluminosilicate gel. Also, hydrolytic attack, in which water molecules break the Si-O-Si structures, can be the cause of low durability of the geopolymer matrix.

The thermodynamic models developed with different mix designs and varying

doses of FGD wastewater showed that low strength chemical species formed as a result of reaction between the geopolymer gel and anion-saturated wastewater cause discontinuity in the tetrahedral chains in alkali-activated fly ash (geopolymer). These species include Alunite $KAl_3(SO_4)_2(OH)_6$, anhydrite $CaSO_4$, thenardite Na_2SO_4 and halite (NaCl). Moreover, the water-soluble species like thenardite and halite cause disintegration of samples in aqueous environment. On the other hand, the formation of these species result in decrease in charge-balancing ions (Na^+, K^+ and Ca^{2+}) that help in the formation of zeolites. Addition of fly ash type C improved the integrity of the material by formation of species similar to the ones found in hydrated portland cement like calcium silicate hydrate ($C-S-H$), calcium (alkali) aluminosilicate hydrate ($C-(N-)A-S-H$) and Fe monocarbonate ($C3FH6$). These results are in agreement with the models developed by previous studies with alkali-activated blast furnace slag and naturally-occurring zeolites in saline-alkaline lakes and cavities of mafic rocks.

ACKNOWLEDGMENTS

To my better half and restless cheerleader; Simin: because I owe it all to you. Many Thanks!

I owe this success to a whole host of other people. I would like to thank my advisor, Dr. Jy Wu who has always helped me both with administrative and scientific aspects of my studies. I cannot find words to express my gratitude towards my co-advisor, Dr. Langley, and committee members, Dr. John Diemer, Dr. Haitao Zhang and Dr. Churlzu Lim who helped improve my dissertation greatly with their invaluable comments and suggestions.

I am grateful to my parents, Mehdi and Molook, and my sister, Maryam, who have provided me with moral, emotional and financial support throughout all these years. This, would have remained a dream without your help. I am also grateful to my other family members and friends who have supported me along the way.

I would also like to thank Terracon Consulting Engineers and Scientists, especially Mr. Michael Schrum, regional manager, for supporting my last semester of studies.

Last, but by no means least, a very special gratitude goes out to Steve and Linda Waldner. You are like family to me. I appreciate all your support and prayers.

TABLE OF CONTENTS

LIST OF FIGURES

LIST OF TABLES

CHAPTER 1: INTRODUCTION

1.1 Background

Geopolymers are synthetic monoliths with chemical composition similar to natural zeolites. However, X-ray diffraction studies show that unlike zeolites, the microstructure of geopolymers is mostly amorphous [14, 17, 18]. During the process of geopolymerization, Al and Si species in the fly ash, or other aluminosilicate sources, dissolve in the alkaline environment and then condensate to form a quadhedral 3D structure. Cations from the activating alkali solution (Na^+ or K^+), which is made by mixing sodium or potassium hydroxide and sodium silicate or other sources of soluble silicate, balance the charges in the structure formed [77, 78]. High compressive strength, resistance to chemical attacks and, especially, low permeability are characteristics that make geopolymers desirable for immobilization of waste materials [17]. The immobilization of municipal waste incineration residue was successful in geopolymers made with blast furnace slag [30]. Also, despite their low compressive strength (less than 1 MPa or 145 psi), geopolymers made with metakaolin and potassium silicate showed good sequestration performance [30]. The results of European leaching

compliance test for granular waste materials and sludges (UNE-EN 12457) on the leachates of these samples, showed that the concentration of all metals except for Sb, were in non-hazardous waste limit. Also, Toxicity Characterization Leaching Procedure (TCLP) [22] generally had good results. The results of these tests show that although a significant release of Mo, V, Sb and Ba was observed, the concentration of these metals was always lower than USEPA (United States Environmental Protection Agency) limits [30]. Tank leaching test NEN 7345 (Leaching characteristics of soil, construction materials and wastes leaching tests) the lowest concentration of Zn and Cr was released from geopolymeric samples made with blast furnace slag compared to metakaolin geopolymers, OPC (ordinary Portland cement) and OPC with lime systems [30]. Stabilization of carbon electric arc furnace residues with geopolymerization technique was also successful [69]. Best results were achieved after 28 days in geopolymers made with potassium silicate and blast furnace slag [69]. In this case, UNE-EN 12457 test on the potassium silicate geopolymer leachate resulted in 0.9, less than 2 and 0.6 mg/Kg for Zn, Pb and Cr, respectively, which was much lower than the amount leached from OPC samples (17, 300 and 35 mg/Kg respectively). Also, Cd concentrations were lower than detection limit for all geopolymer samples. TCLP tests show that geopolymer leachates had neutral pH between 5.2 and 6.7. Moreover, although both OPC and geopolymer leachates met the USEPA limits,

geopolymers stabilized Cr better (less than 0.05 as compared to 2.7 mg/L for OPC). NEN 7345 tank leaching test also revealed that geopolymeric immobilization techniques result in lower metal leaching than OPC samples [69]. Other authors have also worked on immobilization of several metal anions in different systems including geopolymer structures [28, 43, 70, 83].

There have been numerous research articles discussing the possibility of sequestration and reducing the leaching from coal combustion byproducts. Cetin et. al. [9] studied leaching of metals from high carbon fly ash highway bases stabilized by lime kiln dust (LKD). A first flush pattern was observed but all the metals except Al returned to their allowable levels for USEPA maximum concentration limits for drinking waters (MCLs), EPA water quality limits (WQLs) and Maryland aquatic toxicity limits for fresh water (ATLs) . Oxyanions leaching from fly ash stabilized by calcined and partially calcined dolomite additive was studied by Guo and Readon [36]. Due to lower alkalinity and calcium concentration, partially calcined dolomite (PCD) showed better immobilizing effect. Anions (Cl^-, CO_3^{2-}, $C_2O_4^{2-}$ and PO_4^{3-}) interrupt the formation of aluminosilicate gel by the formation of precipitates and crystals. Chloride is specifically thought to be the primary cause of this process and the compressive strength is decreased [55, 53]. However, carbonate salts (K_2CO_3 and $CaCO_3$) prevents hydrolytic attacks on the gels by decreasing the dissolved water

[55, 53]. Hydrolytic attacks on the geopolymer gel [10] could be an underlying cause of low compressive strength in samples made with wastewater. This phenomenon will be explained in detail in the upcoming sections.

1.2 Problem Statement

Flue gas desulfurization wastewater, containing high concentration of halides and heavy metals, poses a threat to environmental safety including bodies of drinking water and soil. The release of this waste stream through leaching to the groundwater or spillage to bodies of water near power plants, increases the chance of trihalomethane formation that are known carcinogens. Efforts were made to sequester this waste stream in solid matrices according to EPA recommendation. During the experimental phase of this research, efforts to use fly ash type F geopolymer matrix to sequester the brine were not successful because FGD wastewater caused the matrix to disintegrate. Moreover, the resulting species of the mix designs using different percentages of fly ash types F and/or C, activator solution and wastewater are not clear due to complex chemical reactions. On the other hand, efforts to mix the brine with the activator solution resulted in precipitation. Hence, thermodynamic modeling of the chemical reactions can clarify the cause of these phenomena by determining the nature and amounts of resulting species in the phase assemblages.

1.3 Research Objective

The primary goal of this research is to understand the species formed during the sequestration of halides using geopolymer matrix. The key objectives of this dissertation are:

- Modeling geopolymer chemistry with different percentages of FGD wastewater and characterizing the mineralogy.
- Identifying the cause of failure in the geopolymer matrix due to inclusion of halides.
- Providing a tool to explain and predict the matrix behavior based on the models developed.

When completed, the results of this research can lead to a better practical tool to predict the behavior of the sequestration material with a given mix design.

1.4 Research Hypothesis

The hypothetical impacts of the ion-rich brine on the geopolymer matrix would include the following:

1. Cations play the charge balancing role in addition to Na^+ and/or K^+ and reduce the workability of the fresh paste and induce flash setting [52, 20, 15].

2. The presence of calcium will start a competing process with the geopolymerization to use OH^- ions to produce $C-S-H$ [37, 38].

3. The silalate-siloxo chain in geopolymer can be interrupted by unreacted particles, crystalline species or other impurities from either fly ash or brine.

4. The reactions of anions with charge-balancing ions (Na^+, K^+ and Ca^{2+}) could form species that reduce the concentration of these charge-balancing ions and terminate or slow down the geopolymerization process.

5. Durability issues might arise due to the presence of water and hydrolytic attack [53] [75]:

$$\equiv Si-O^-Na^+ + HOH \rightarrow \equiv Si-OH + Na^+ + OH^- \quad (1)$$

$$\equiv Si-O-Si \equiv +OH^- \rightarrow \quad \equiv Si-OH + \equiv Si-O^- \quad (2)$$

$$\equiv Si-O^- + HOH \rightarrow \quad \equiv Si-OH + OH^- \quad (3)$$

The addition of calcium ion either in the form of CaO, $Ca(OH)_2$ or $CaSO_4$ to the geopolymer paste is known to shorten the set time of the pastes. The cations (Ca^{2+}) can act as charge balancers like Na^+ and K^+ [15]. When there is higher charge balancer amounts in the system it will result in faster geopolymer formation. On the other hand, the dissolution rate of calcium silicate glasses is higher compared to

higher silicate concentrations. Therefore, the silicate needed for network formation is available faster [20]. Also, calcium reacts very quickly with silicon and aluminum in aquatic environment and form calcium silicate hydrate ($C-S-H$) and calcium aluminate hydrate ($C-A-H$); reactions similar to the hydration of ordinary Portland cement and calcium aluminate cement. In the geopolymerization gel, due to the presence of soluble aluminum and silicon species, this reaction happens even faster [21]. There is evidence that the $C-S-H$ and geopolymer phases coexist in the mix but their ratio changes depending on the alkalinity of the environment and available soluble calcium amount [84]. The reactions involving geopolymer precursor and geopolymer backbone is presented here [82].

$$CaO + H_2O \rightarrow Ca(OH)_2 \rightarrow Ca^{2+} + 2(OH)^- \quad (Dissolution\ of\ Ca\ in\ water) \quad (4)$$

$$n(Si_2O_5, Al_2O_2) + 2nSiO_2 + 4nH_2O + NaOH(Ca(OH)_2 or KOH) \rightarrow$$

$$Ca^{2+}, Na^+, K^+ + n(OH)_3 - Si - O - Al^-(OH)_2 - O - Si - (OH)_3$$

$(Dissolution\ of\ Al\ and\ Si\ species\ in\ alkalin\ environment\ and\ their\ interlinking)$

(5)

$$n(OH)_3 - Si - O - Al^{-}(OH)_2 - O - Si - (OH)_3 + NaOH(Ca(OH)_2 or KOH) \rightarrow$$

$$(Ca^{2+}, Na^{+}, K^{+}) - (-Si - O - Al^{-} - O - Si - O-) + 4nH_2O$$

$$(Charge\ balancing) \quad (6)$$

$$6Ca^{2+} + 2Si^{4+} \rightarrow 3CaO \cdot 2SiO_2 \cdot 4H2O + 3Ca(OH)_2 \qquad (in\ aquatic\ environment)$$

$$(The\ formation\ of\ Calcium\ Silicate\ Hydrate) \quad (7)$$

When the alkalinity of the environment is high, the excessive OH^{-} ion is not in favor of equation 4. So, the calcium ions cannot be dissolved in the environment. Therefore, the geopolymer phase becomes dominant and $C-S-H$ phase is developed after the geopolymer final network is developed. As a result, the $C-S-H$ phase fills the voids of the geopolymer matrix and improves its mechanical properties [20, 38, 21, 51, 57, 60, 1]. Low alkalinity of the solution provides the opportunity for CaO to react with water and be ionized. This reaction will make the $C-S-H$ phase become dominant in the matrix.

Based on equation 4, the presence of CaO increases the pH of the pore solution and as explained before, increases the $C-S-H$ phase in the matrix. The compact structure of $C-S-H$ geopolymer composite matrix and the opportunity for the metal ions to be chemically bonded or physically encapsulated in the matrix seems to be in favor of metal sequestration. It is shown that the geopolymer matrix is a

viable solution for almost 100% sequestration of As, Se, Fe and Zr [17, 1] and Br [29].

Excessive amount of CaO will induce flash set in geopolymer matrix which will affect the workability of the material. This behavior is affected by the availability of silica and alumina as well as the alkalinity of the solution. Experimentally-controlled amount of CaO and solution alkalinity level can provide an optimum mix design. However, as many of these factors are interrelated, determining this optimum is a difficult job. For this purpose, mix designs are proposed in the initial trial and error study stage and the workability, setting temperature and setting time are checked.

1.5 Research Scope

The premise of this research is to understand the chemistry of geopolymer matrix contaminated by varying doses of halides from FGD wastewater. This purpose is realized by modeling the matrix using thermodynamic tools. The data from the initial experimental works helps validate the model results. Also, the model can help understand the reason behind the failure in some of the experimental works. The focus of the research is limited to the contamination of halides not other contaminants in geopolymer matrix. The chemical speciation models are developed using the Gibbs energy minimization modeling technique.

1.6 Organization

The remainder of this research dissertation consists of four other chapters. Chapter two is dedicated to some background information regarding coal combustion byproducts and their disposal, Gibbs minimization modeling and state-of-the-art in studies regarding the modeling of solid phases especially halides. In chapter three, the experimental and modeling phases of the study are laid out. The methods used for thermodynamic modeling of the sequestration material phases are explained fully in this chapter. In chapter four, the leachability test results and models for each mix group is presented and interpreted. Finally, in chapter five, a summary of the research is presented and the results are elaborated further.

CHAPTER 2: LITERATURE REVIEW

2.1 Coal combustion byproducts

Coal combustion byproducts consist of the material left after combustion from power plants using coal as a fuel. These materials include fly ash, bottom ash, boiler slag and flue gas desulfurization or FGD. Various air pollution control devices are used to collect these byproducts. Depending on factors including the operating temperature of the boiler , the type of pollution control device , the coal chemistry and pre-use condition and chemistry of the coal, the chemistry of the byproducts Change. Typical ranges of constituents of these byproducts are given in tables 1 and 2.

The most abundant byproducts of coal combustion are fly ash and FGD Material. Fly ash is the output of particulate control devices. These devices include electrostatic precipitation, fabric filtration, scrubbers, mechanical centrifugal systems and gaseous emission control devices. Gaseous emission control devices are used to control the gas phase of the contaminants and particulates smaller than 1 micrometer. The most common particulate control system is electrostatic precipitation system.

Table 1: Typical constituents concentration in FGD wastewater

Component	Unit	Concentration
Cl^-	mg/Kg	94075
Br^-	mg/Kg	2800
NO_3^-	mg/Kg	760
SO_4^{2-}	mg/Kg	11070
B	mg/L	147
Cr	mg/L	0.9
Mn	mg/L	0.14
Ni	mg/L	0.02
$Zinc$	mg/L	2.12
As	mg/L	0.8
Se	mg/L	31.4
Mo	mg/L	0.01
Cd	mg/L	5.6

Table 2: Typical constituents concentration in fly ash types F and C

Component	Unit	Fly Ash F	Fly Ash C
F^-	mg/Kg	2.37	12.71
Cl^-	mg/Kg	2.41	2.06
Br^-	mg/Kg	0.1	0.1
NO_3^-	mg/Kg	0.32	0.125
SO_4^{2-}	mg/Kg	1194	1.25
Al_2O_3	Wt%	28.7	19.2
BaO	Wt%	0.07	0.07
CaO	Wt%	1.9	23.3
Fe_2O_3	Wt%	7	6.2
K_2O	Wt%	0.8	0.8
MgO	Wt%	1.49	1.5
Na_2O	Wt%	1.7	1.7
P_2O_5	Wt%	0.5	0.5
SiO_2	Wt%	51.9	39.3
SrO	Wt%	0.1	0.1

Fly ash is the product of particulate control systems. The chemistry of fly ash can be different depending on the coal type, the operating temperature of the boiler, and emission control regulations. There are two main classes of fly ash that have different properties. Class F fly ash is the result of burning lignite or bituminous coal. It has lower calcium content (6% or less CaO by weight) and no self-cementitious properties. Class C fly ash, on the other hand, is the result of burning lignite or sub-bituminous coal. The amount of CaO is generally above 15% by weight. It has both pozzolanic and self-cementotious properties.

FGD material is the product of desulfurization technology. This technology is utilized to capture gaseous and sulfur oxides from flue gas using gaseous emission control devices. The objective of this research is to use these two prominent byproducts of coal combustion (FGD and fly ash) to provide a better solution for disposing of them safely.

2.2 FGD material

FGD waste is the second most abundant coal combustion byproduct with 22.7 million metric tons of annual production. This material consists of dewatered scrubber sludge and some fly ash. Scrubber sludge is the result of exposing the flue gas to an aqueous solution of lime or limestone as sorbent. Alternatively, the scrub-

ber technology can use sodium hydroxide or sodium sulfite as absorbent solution in dual-alkali scrubber technology. The former technology results in calcium sulfite or calcium sulfate or a mixture of both; whereas the latter generates calcium sulfite and sodium salts. Moreover, in spray-drying scrubber systems, sodium-based reagents are used to produce sodium sulfate and sodium sulfite. The main components of FGD material are calcium and sulfur. The calcium content (as CaO, gypsum or calcium sulfite) ranges from 10% to 30% depending on the scrubber technology while the sulfur (mostly as sulfate or sulfite salts) content may range from 2 to 11%.

The most common absorbent used the United States is lime and limestone. As stated before, the main products of this kind of system are calcium sulfite and calcium sulfate. Calcium sulfate or gypsum is used in sheet rocks, agricultural purposes, soil remediation purposes and Portland cement production whereas calcium sulfite or gypsite has no specific market and is usually landfilled.

FGD material also contains detectable amounts of arsenic, cadmium, chromium, copper, lead, molybdenum, nickel, selenium and zinc as well as halides mostly chloride and bromide. Although toxicity characteristics leaching procedure (TCLP) tests by EPA shows low amounts of these constituents, the main concern is the leaching and accumulation of these elements in surface and groundwater. Moreover, EPA assessment is mostly concerned with disposal in landfills. Utilities dispose of these

materials in surface impoundments which can cause uncertainty in terms of its impact on long-term human and environmental health. Thus, safe disposal of FGD material by sequestration is a necessary step towards environmental risk management. Understanding the produced phases using modeling tools can clarify the reason behind the behavior of the material.

2.3 Disposal of Coal Combustion Byproducts

Disposing of coal combustion byproducts has become a challenge for the countries using coal as fuel for electricity generation. The common practice of accumulating these byproducts in slurry containment ponds near the power plants has proved to be problematic due to several spill incidents to the aquatic environments including the recent incident into Dan River on February the 2nd 2014 [42]. Due to aging ponds (some of them are as old as 75 years in the US), as well as more strict regulations by EPA to eliminate toxic byproducts from the emissions, this problem has become more evident. It has been estimated that 134 million tons of coal combustion byproducts were generated in the US by 460 coal power plants. 47% of this amount is coal fly ash. 38 million tons of fly ash has been landfilled [4].

One of the most toxic coal combustion byproducts comes from a process called flue gas desulphurization. In this process, SO_2, the acid rain precursor, is removed from the emissions [32]. Flue gas desulphurization process (wet scrubber) removes

Table 3: Concentration of Anions in Bowen FGD Fly Ash

Anions	Concentration (ppm)
Fluoride	<0.125
Chloride	86,000
Bromide	2,700
Nitrate	77
Phosphate	<0.10
Sulfate	3,730

70 to 90% of the SO_2 in the flue gas. Wet limestone FGD process is preferred due to its high efficiency, low energy use and reliability [48] where SO_2 gets absorbed to limestone slurry and then the slurry is dewatered [62]. The wastewater produced from this process is called FGD brine and the spray-dried solid part, which contains halides (Cl^-, F^- and Br^-), sulfate, nitrate and phosphate is called FGD fly ash. Recent restrictions on coal combustion emissions have led to the accumulation of several toxic materials in fly ash and FGD [32]. The concentration of anions in FGD fly ash is shown in Table 3. Statistics show that since 1970s, 100 million tons of FGD fly ash was produced in Europe [56].

There have been numerous research articles discussing the possibility of sequestration and decreasing the leaching from these byproducts. Cetin et. al. studied leaching of metals from high carbon fly ash highway bases stabilized by lime kiln dust (LKD). A first flush pattern was observed but all the metals returned to their allowable levels except for Al [9]. Oxyanions leaching from fly ash stabilized by cal-

cined dolomite additive was studied by Guo and Readon. Due to lower alkalinity and calcium concentration, partially calcined dolomite (PCD) showed better immobilizing effect [36]. Leachability of certain fly ash elements is pH-sensitive. The fly ash pH is, in turn, controlled by the ratio between Ca and S [44].

Stabilization of different solid wastes in geopolymer systems has been studied [30, 69]. Geopolymers are synthetic monoliths with chemical composition similar to natural zeolites. However, X-ray diffraction studies shows that unlike zeolites, the microstructure of geopolymers is mostly amorphous (Figure 1) [17, 18]. During the process of geopolymerization, Al and Si species in the fly ash, or other aluminosilicate source, dissolve in the alkaline environment and then condensate to form a quadhedral 3D structure. Cations from the activating alkali solution (Na+ or K+), which is made by mixing sodium or potassium hydroxide and sodium silicate, balance the charges in the structure formed [77, 78]. High compressive strength, resistance to chemical attacks and especially, low permeability are characteristics that make geopolymers desirable for immobilization of waste materials [17]. The immobilization of municipal waste incineration residue was successfully done in geopolymers made with blast furnace slag. Also, despite their low compressive strength, geopolymers made with metakaolin and potassium silicate showed good sequestration performance [30]. Stabilization of carbon electric arc furnace residues with geopolymer-

ization technique was also successful. Best results were achieved after 28 days in geopolymers made with potassium silicate and blast furnace slag at 60 degrees Celsius [69]. Other authors have also worked on immobilization of several metal anions in different systems including geopolymer structures [28, 43, 70, 83] but to the best of our knowledge, nobody has tried to immobilize FGD fly ash in geopolymers.

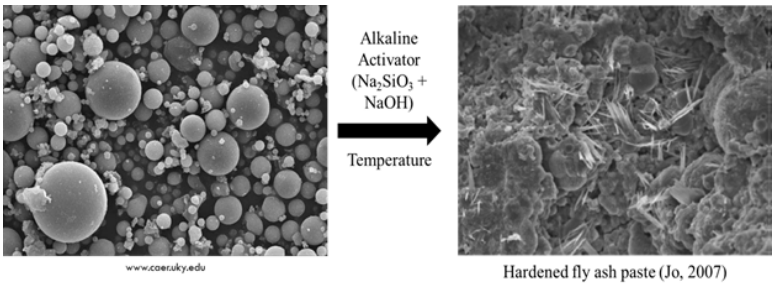

Figure 1: Fly Ash Geopolymerization

2.4 Geopolymerization Process

Understanding the geopolymerization process during which the geopolymer matrix is developed, can help understand the chemistry of the sequestered material as well as the behavior of the matrix in contact with the waste material. The polycondensation of the groups from the polymerization stage results in the formation of aluminosilicate oligomers with sialate ($-Si-O-Al-O-$) groups [15, 12]. In the polymerization stage, tetrahedral structure consisting of random Si and Al atoms is formed by crosslinking between the sialate groups. Ions of Na^+, K^+ or Ca^{2+} are located in the cavities to provide charge balance [74]. It is known that the crosslinking starts with

intermediate aluminum-rich species with low energy $Al-O-Al$ bonds and then are interlinked more by Si [5]. This happens because the dissolution rate of Al is higher than Si [38, 23, 26, 67, 79, 24]. The availability of silica in the activating solution starts the interlinking earlier and gives time to the dissolution of Si from fly ash particles. Also, studies show that the presence of a readily available soluble silicate source in this stage inhibits the formation of nanocrystalline zeolite structures such as hydrosodalite, chabazite-Na and gismondine in later stages of geopolymerization. It is believed that the high water/solid ratio of 1 in this case (compared to 0.3) plays an important role in crystallization of the system [5].

With increase in the crosslinking degree, the dissolution rate is decreased due to the geopolymer network covering the unreacted amorphous fly ash and hence, unavailability of the base material. Also, the amount of available hydroxide ion decreases which decreases the dissolution rate further [24]. During the final stage, the curing temperature increases the rate of $Si-O-Si$ dissolution and breaks the small networks to form larger ones. Also, some $Al-O-Si$ bonds might be broken and replaced by $Si-O-Si$ bonds [79].

Although the chemical composition of coal fly ash can differ slightly based on several factors including the source coal, combustion and cooling conditions and overall furnace configuration; it generally consists of a good source of amorphous

aluminosilicate for fly ash geopolymer fabrication. It also has crystalline species of which quartz (SiO_2), mullite ($3Al_2O_3 \cdot SiO_2$), hematite (Fe_2O_3) and maghemite ($\gamma - Fe_2O_3$) are more quantifiable. The crystalline phase of fly ash reacts with the alkaline activator in a much slower rate than the amorphous phase [15, 35] and is usually considered as the unreactive portion and hence, part of the impurities of it. Also, the amorphous phases trapped in crystalline shells cannot react with the activator due to the crystalline barrier. Therefore, although X-ray Diffraction (XRD) technique can give an almost accurate estimation of the crystalline and amorphous phases of the base material, it does not necessarily determine the reactive portion. In other words, the reactive portion of fly ash is less than what is determined as the amorphous phase [26, 39].

In order to tackle this problem, Chen-Tan et. al. (2009) [11] proposed to use a technique called $NaOH$ chemical attack. In this technique, a small amount of the fly ash sample is dissolved in aqueous sodium hydroxide and agitated at a fixed temperature. Due to high ratio of $NaOH$ to fly ash, no aluminosilicate species will be formed. The solution is then filtered and the unreacted fly ash is washed, dried and weighed. The results are compared and correlated with the X-ray Fluorescence (XRF) and XRD results. The percent weight of the reactive source material is taken into consideration for model development.

The cured geopolymer consists of tetrahedral poly(sialate), poly(sialate-siloxo) and poly(sialate-disoloxo) structures. These structures can be developed according to the availability of the building blocks. Figure 2 shows the structures that can occur based on the ratio of Si/Al. Theoretically, the backbone of these structures is polysilane which is unstable and cannot be found in natural form. These structures are formed during the polycondensation of the amorphous silica and alumina. These amorphous species can be inherited from dissolved fly ash particles or readily available silica from the activator solution (specifically sodium silicate) [15, 16]. The amorphous phase can be characterized using conventional characterization methods like x-ray diffraction (XRD), x-ray fluorescence (XRF) and energy-dispersive x-ray spectroscopy (EDX) on scanning electron microscope.

The data from XRD are used to estimate the ratio of amorphous and crystalline phases [72]. It is expected to achieve a spectrum consisting of crystalline structure in an amorphous matrix (peaks on an amorphous hump). X-ray fluorescence is used to understand the elemental composition of the bulk material. The data from the x-ray diffraction can be used to estimate the amount of the amorphous and crystalline phases. In order to understand the empirical formula, the sample can be digested in acid and analyzed using inductively coupled plasma mass spectrometry (ICP-MS). In this characterization method, the sample is ionized using plasma and a detector

will quantify the dispersed ions. In the end, EDX on scanning electron microscope is used to pinpoint different morphology and their respective elemental composition.

2.5 The effect of halide contamination on geopolymerization

Several studies have focused on the effects of inorganic salt contamination, especially chloride, on the strength and durability of geopolymers. The main processes that affect the geopolymerization process include precipitation of secondary crystals due to the presence of contaminants and hydrolytic attack (water attack).

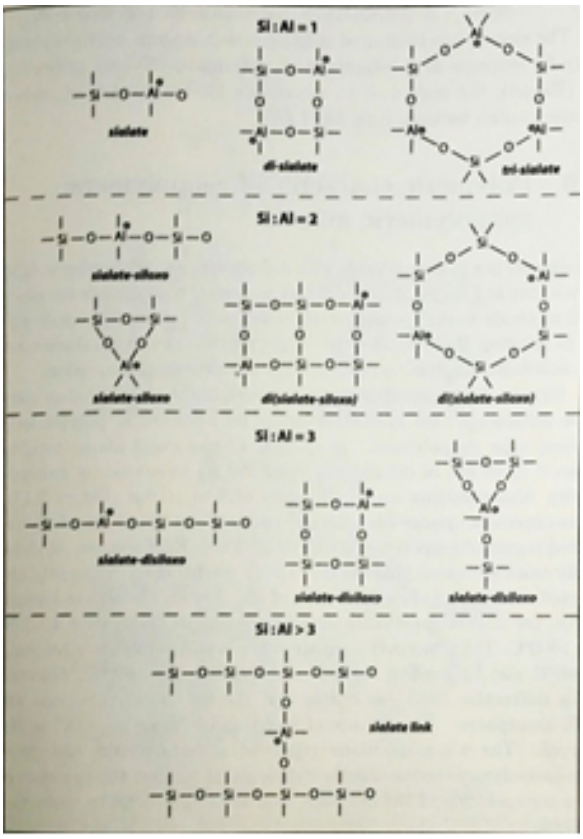

Figure 2: Poly(sialate) geopolymers based on the ratio of Si:Al [15]

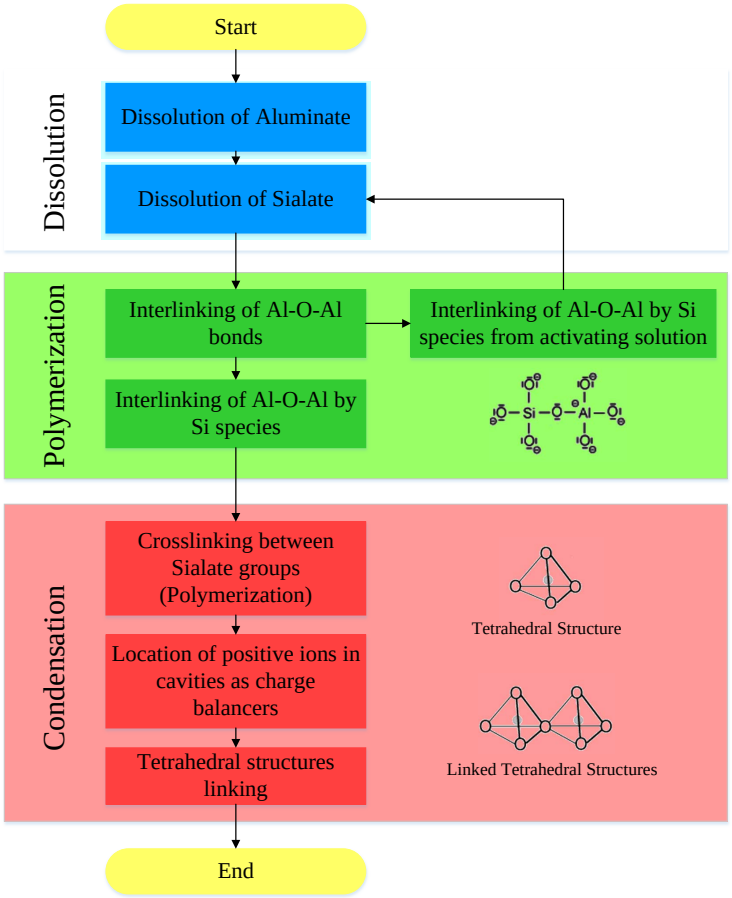

Figure 3: Geopolymerization process flowchart [15]

A study performed on the effect of inorganic salt contamination on the strength and durability of geopolymers showed that chloride-induced crystallization caused discontinuity within the aluminosilicate gel. The crystalline phase replaced the dissolved fly ash particles in high-alkaline systems [53]. Another study performed by Lee et. al. showed that despite higher early strength gains in the presence of chloride, the

durability of the samples were jeopardized due to debounding of interfacial transition zone caused by precipitation [54]. Local formation of hydroxide precipitates, caused by the double charged cation salts contamination (like Ca^{2+} and Mg^{2+}), lowers the pH level and triggers nucleation and early setting [52]. A mathematical model simulating geopolymerization showed that anions including chloride and carbonate affect the chemistry as well as the geopolymerization process. It was also observed that chloride salts can retard the geopolymerization process by decreasing the rate of the Si secondary precipitation. The long-term effects of the salts on the geopolymers were not studied [55]. In a study for immobilization of municipal solid waste fly ash, it was observed that water-wash pretreatment of the fly ash increased the early strength of geopolymer from 15 MPa in case of untreated samples to 23 MPa in case of water-washed geopolymer. It was shown that the pretreatment contributed to decrease in chloride species content of geopolymer [85]. XRD studies also showed that CaClOH was eliminated by converting to $Ca(OH)_2$ and then $CaCO_3$ through the following processes:

$$CaClOH + NaOH \rightarrow Ca(OH)_2 + NaCl \tag{8}$$

$$Ca(OH)_2 + CO_2 \rightarrow CaCO_3 + H_2O \tag{9}$$

The occurance of Ettringite ($Ca_6Al_2(SO_4)_3(OH)_{12}.26(H_2O)$) was observed in untreated geopolymer and was eliminated by water-wash pretreatment. Also, this treatment decreased the depolymerization process during leaching test [85].

In Lee et. al. study, the presence of water or hydroxyl groups in chloride-contaminated mixes caused lower compressive strength. High basicity due to higher Na^+ mobility was shown to affect bridging and non-bridging oxygen. This, in turn, makes T-O-Si more reactive and susceptible to hydrolytic attack [53] [75]:

$$\equiv Si - O^- Na^+ + HOH \rightarrow \equiv Si - OH + Na^+ + OH^- \tag{10}$$

$$\equiv Si - O - Si \equiv + OH^- \rightarrow \quad \equiv Si - OH + \equiv Si - O^- \tag{11}$$

$$\equiv Si - O^- + HOH \rightarrow \quad \equiv Si - OH + OH^- \tag{12}$$

The use of carbonate salts were shown to reduce water and/or hydroxyl content in the gel and increase strength [85].

2.6 Gibbs energy minimization modeling

The present research uses Gibbs energy minimization modeling to produce phase diagrams. The center point of this modeling tool is Gibbs function shown below.

$$G = H - TS \tag{13}$$

Where H is the enthalpy, T is temperature and S represents entropy. This function is used to understand if the system is in equilibrium at a given stage. Also, it can be used to understand at what chemical composition the system reaches the state of equilibrium. In this method, the Gibbs free energy of the system is set equal to zero. In a system with n components, this is done for each component separately. The free energy has three terms; the fusion term, the free energy of mixing of the liquid solution and the free energy of mixing of the solid solution. These terms are explained in detail in next chapter. In systems with several components, like the one the subject of this research, the calculations can easily get complicated. For this reason, computer software is used to model the system. In this Study, GEM-Selektor software package was used for modeling. GEMS considers all gaseous, aqueous, liquid, solid or surface species as independent components. The total molar quantity of the materials in the system in the bulk composition is considered separately. The stability of species at a specific temperature and pressure is defined by its standard molar Gibbs energy function. The Gibbs energies together with the activity terms in the respective phases compose primal chemical potentials then multiplied by X_j and summed up into the total Gibbs energy of the whole system. Then the software

calculates the X_j's that minimize the total energy.

The occurrence of product phases in an alkali-activated slag system was analyzed by changing certain ingredient masses using thermodynamic modeling by GEMS Selektor 3.3 [66]. The extended modeling on the Myers models performed by the author include CaO, MgO and SiO_2. Resultant phases in different sensitivity analyses include Brucite (MH), Straetlingite (C_2ASH_8), $MgAl-OH-LDH$ and $C-N-A-S-H$. These phases are studied separately in the following phase diagrams.

The occurrence of the aforementioned solid phases with increase in the CaO content is shown in Figure 4 As it can be seen, increase in CaO content naturally increases the $C-N-A-S-H$ phase because calcium is one of the building blocks of $C-N-A-S-H$ phase. Brucite was not observed in this case. $MgAl-OH-LDH$ phase does not change greatly here because the amount of Mg is kept constant during the simulation. Increase in the amount of CaO to 21 grams triggers the appearance of straetlingite which decreases $CNASH$ phase.

The solid phase assemblage was also simulated with increasing amounts of MgO (Figure 5). In this case, the increase in MgO increased the $MgAl-OH-LDH$ phase which was expected. The maximum amount of this phase is observed at 17.6 mass percent MgO. Straetlingite forms at the beginning of the simulation at 1 to 7

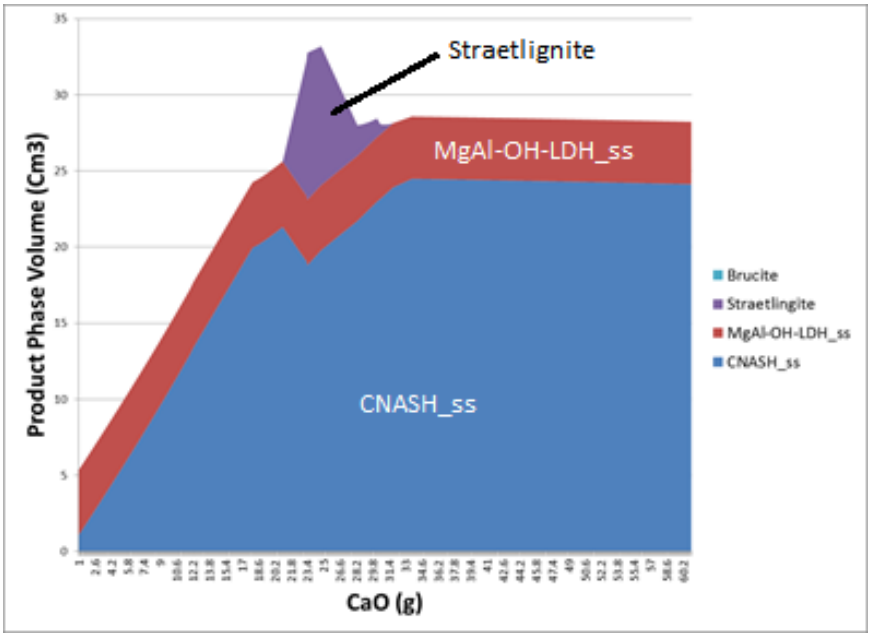

Figure 4: Simulated solid phase assemblages with increase in CaO content

mass percent MgO. Also, brucite forms at 13.2 mass percent MgO. This happens due to increase in Mg/Al ratio and the surplus Mg that did not enter the reaction to produce $MgAl - OH - LDH$, produces brucite.

Figure 6 shows simulated solid phase assemblage with increase in SiO_2 content. Again, as it is expected, with increase in the amount of Si, $C - N - A - S - H$ phase increases in this case. $MgAl - OH - LDH$ phase does not change greatly in this case because Mg/Al ratio is kept constant during the simulation. Straetlingite phase forms between 17 and 29 mass percent of SiO_2. This point of the graph corresponds to a decrease in the slope of $C - N - A - S - H$ phase. Brucite phase did not form in this simulation.

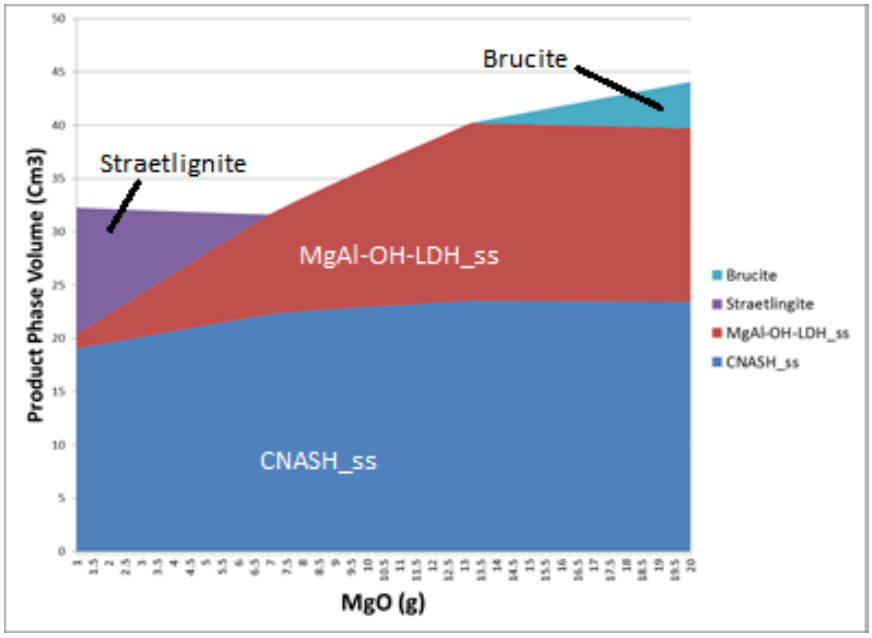

Figure 5: Simulated solid phase assemblages with increase in MgO content

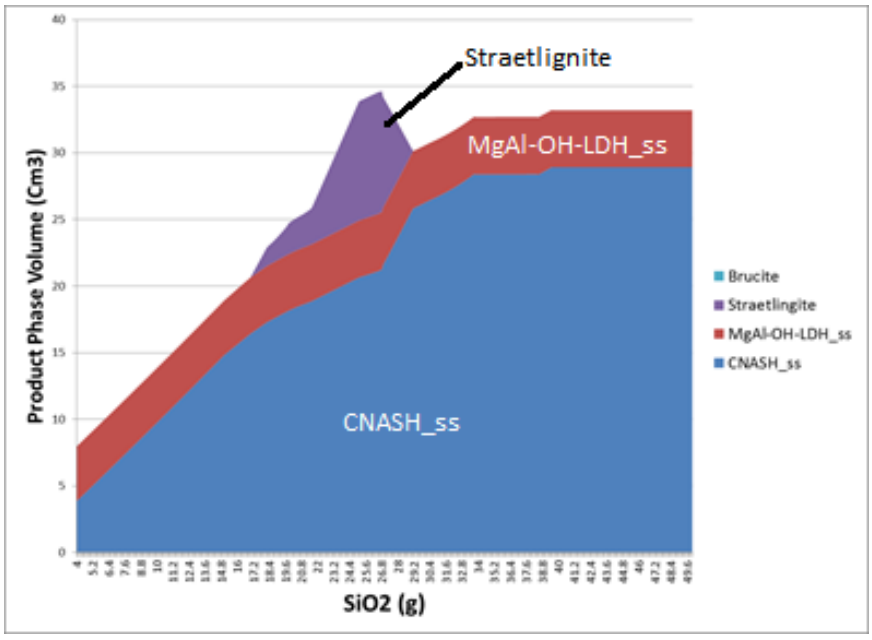

Figure 6: Simulated solid phase assemblages with increase in MgO content

CHAPTER 3: RESEARCH METHOD

In this chapter, the methodology used to achieve the objectives of the research is discussed in detail. The research will consist of three main phases which are discussed separately. The completion of each phase provides data and material to start the next phase and play as a prerequisite for the rest of the research. In the first section, the experimental procedures to acquire the data for the modeling phase are presented. Moreover, a part of the acquired data will be set aside for the validation phase. In the second phase, the input data will be used to develop the model using thermodynamic modeling tools to figure out the equilibrium phases. The model will be verified and validated in the third phase using the additional data obtained in the first phase.

3.1 Phase One: Experimental Phase

The experimental phase of the research needs a meticulous study on the independent variables affecting the chemical phases in the geopolymer. In this regard, the chemistry of the fly ash and FGD material can play the primary role. Also, the mix design of the sequestration materials developed and the procedures used are

considered to provide the most accurate input data for the modeling phase.

3.1.1 Materials

The fly ash class F and class C were obtained from plant Bowen and plant Scherer respectively. Also, for this study, a synthesized brine solution as a substitute to concentrated FGD wastewater (WW) was provided by Southern Company in Georgia. ZLD dry salt from plant Bowen was used in some samples. For the activator solution, NaOH pellets were provided by UNIVAR and sodium silicate was obtained from Oxychem.

3.1.2 Mix Designs

The following mixes (Table 4) were prepared using a tabletop mixer. The F-slurry, containing class F fly ash and activator solution, was made in the first step. The activator solution consisted of a mixture of sodium hydroxide ($NaOH$) and sodium silicate ($NaSiO_3$) with $NaOH : NaSiO_3$ ratio of 0.13. In the next step, if needed, the slurry underwent vacuum. Then, wastewater was added to the mix. For some of the mixes (S3.3 to S9.4), different compaction energy was applied to the mix. All the samples were cured for 24 hours before leaching test. The samples made with fly ash type F and more than 20% wastewater content had inadequate strength to proceed with the leaching test.

In case of FVC samples (vacuumed fly ash F slurry with fly ash C), the F slurry

Table 4: Geopolymer recipes and techniques

	Class C Content	Activator Content	F/C Ratio	Wastewater Content	Vacuum	No Class C	Curing Temperature	Vacuum after casting	Compaction
Control	○	○	○	✓	○	✓	○	○	○
A-W-FC00 to A-W-FC15	✓	○	✓	○	○	○	✓	○	○
A-W-FC17 to A-W-FC23	✓	✓	○	○	○	○	✓	○	○
W-FC27	○	○	✓	○	○	○	✓	○	○
W10-FC to W20-FC	✓	○	○	✓	○	○	○	○	○
W30-FC	✓	○	○	✓	○	○	○	○	○
W20-FC *	✓	○	○	✓	○	○	○	○	○
W35-FC *	✓	○	○	✓	○	○	○	○	○
W10-FVC to W30-FVC	✓	○	○	✓	✓	○	○	○	○
W10-FV to W20-FV	○	○	○	✓	✓	✓	○	○	○
W10-FVM to W20-FVM	○	○	○	✓	○	✓	○	✓	○
S3.3-C30 to S9.4-C70 *	○	○	○	✓	○	✓	○	○	✓
* These samples were prepared using dry ZLD salt.									

was prepared and put under vacuum for 24 hours before adding the class C fly ash and wastewater and curing. In FVM samples, the mixes were prepared with no class C ash. They were cast in cylindrical molds with lateral 1 mm holes. Then, they were put under vacuum before curing at 75 degrees Celsius.

The mass percentages of the mix components are presented in table 5. The first three samples were cured at both room temperature (RT) and oven temperature (OT). The mixes with * were prepared using dry salt. In order to have a better un-

Table 5: Geopolymer mix designs

Mix Name	Wastewater or Dry Salt	Fly Ash F	Fly Ash C
	%	%	%
Control	0	69	0
W10	10	35	30
W15	15	33	27
S3.7 *	3.7	35	30
S3.3 *	3.3	67	0
S6.5 *	6.5	65	0
S9.4 *	9.4	63	0
W10-FVM	10	65	0
W10-FVC	10	35	30
W15-FVM	10	60	0
W15-FVC	15	33	27
W20-FVM	20	55	0
W20-FVC	20	30	25

derstanding of the equivalency of ZLD (Zero Liquid Discharge) salt and wastewater, the itemized salt components were calculated for each mix design. These values are presented in table 6.

The anion concentration used for calculation of these values was obtained from ion chromatography of wastewater and dry salt (table 7). The analysis provided by the client is presented for comparison purposes and is not used in calculations.

Table 6: Average concentration of anions in the geopolymer recipes

	AVERAGE CONCENTRATION			
	Chloride	Bromide	Nitrate	Sulfate
	mg/Kg	mg/Kg	mg/Kg	mg/Kg
Control	1.66	0.07	0.22	823.89
W10	9408.96	280.07	76.15	1525.29
W15	14112.60	420.06	114.14	2054.87
S3.7 *	11208.02	312.35	43.07	2784.81
S3.3 *	9088.01	253.27	35.01	2718.81
S6.5 *	18174.37	506.47	69.81	4613.73
S9.4 *	27260.72	759.66	104.60	6508.65
W10-FVM	9409.07	280.07	76.21	1883.13
W10-FVC	9408.96	280.07	76.15	1525.29
W15-FVM	14112.70	420.06	114.19	2376.92
W15-FVC	14112.60	420.06	114.14	2054.87
W20-FVM	18816.33	560.06	152.18	2870.72
W20-FVC	18816.24	560.06	152.13	2572.52

Table 7: Anions concentration in wastewater and ZLD salt

Anions	Chloride	Bromide	Nitrate	Sulfate
Unit	ppm	ppm	ppm	ppm
Bowen Wastewater	94,075	2,800	760	11,070
ZLD Salt (IC Analysis)	302,880	8,440	1,160	63,960
ZLD Salt (Provided by Client)	290,000	5,800	77	15,000

3.1.3 Leachability test

EPA leaching LEAF tests (1311, 1313 and 1315) described in [22] were performed on the samples. As the geopolymer matrix was proposed for sequestration of the waste, the monolith should remain intact throughout the leaching test process. Therefore, method 1315 or tank test was considered for the leaching study. In this method, the monoliths were kept in water tanks and the leachate was collected at certain time intervals according to the EPA procedure.

The dominant release mechanism of the analytes at different time intervals can be predicted using the cumulative mass release and mean interval flux for different recipes. The related graphs will be presented in the results section. Based on the slope value, the three dominant release mechanisms are as follows:

- Smaller than 0.35 represents leaching due to surface wash-off or depletion
- 0.35 to 0.65 represents leaching due to diffusion from the monoliths
- 0.65 represents leaching due to dissolution from the monoliths

3.2 Phase Two: Modeling

3.2.1 Gem Selektor Code Algorithm

Gem Selektor 3.0 software package was used for the calculations of phase assemblage and speciation in this thesis [50]. In this section, the basic work flow of the algorithm and the mathematical formulation behind it is explained. White et. al [80] showed for the first time that the equilibrium composition of an complex mixture can be determined by direct minimization of Gibbs free energy without using detailed chemical reactions. In their paper, Gibbs free energy was calculated by summation of the multiplication of $x_{j,k}$ mol quantities of jth dependent component (DC) species and by their respective chemical potential ($v_{j,k}$) as follows:

$$G(x) = \sum_{k} \sum_{j} x_{j,k} v_{j,k} \qquad j \epsilon L_k, k \epsilon \Phi \tag{14}$$

The k index represents the number of phases in the system. The dimensionless chemical potential ($v_{j,k}$) of the jth dependent component in the kth phase is calculated by:

$$v_{j,k} = g_j/RT + lnC_j + ln\gamma_j + Const \qquad j \epsilon L_k \tag{15}$$

In this equation, g_j is the standard Gibbs energy, C_j is concentration as a function of $x_{j,k}$, γ_j is the fugacity (activity) coefficient for the jth dependent component. In 1997, Karpov et. al. [47] introduced the following Gibbs free energy equation for

complex multi-component, multiphase and multiaggregate system:

$$G(x) = \sum_{j\epsilon L} C_j x_j + \sum_{j\epsilon l_k} x_j ln(x_j/X_k) - \sum_{j\epsilon S_w^0} x_j ln(x_{j_w}/X_k) \qquad k\epsilon\phi \tag{16}$$

$$X_k = \sum_{j\epsilon l_k} x_j \tag{17}$$

In this equation, C_j is a function of x_j. The following equations are used to determine the concentration in different phases:

For the solid phase

$$C_j = g_j/RT + ln\gamma_j \qquad j\epsilon L|(S_g U S_w^0) \tag{18}$$

For the gas phase

$$C_j = g_j/RT + ln\gamma_j + lnP \qquad j\epsilon S_g \tag{19}$$

For the aqueous phase

$$C_j = g_j/RT + ln\gamma_j + ln55.51 \qquad j\epsilon S_w^0 \tag{20}$$

In these equations, g_j is the empirical potential function for the j^{th} dependent component in its standard state in constant pressure and temperature. P is the pressure (in bar).

The ultimate goal of Gibbs free energy minimization problem is to minimize $G(x)$.

For this purpose, a vector $\mathbf{x}$ should be found such that:

$$Minimize \quad G(x) \qquad \text{From Eq. 15,} \tag{21}$$

Subject to

$$\mathbf{M1} = \{\mathbf{x}|\mathbf{A}\mathbf{x} = \mathbf{b}, \mathbf{x} \geq 0\} \tag{22}$$

where $\mathbf{x} = \{x_j, j\epsilon L\}$, $\mathbf{A}$ is a matrix containing stoichiometry coefficients and $\mathbf{b}$ contains mole amounts of independent components. In other words, this is the input matrix of bulk chemical composition. Also, the following constraints are imposed on the elements x_j of the speciation vector $\mathbf{x}$:

$$R1 = \left\{ \begin{array}{c} x|x_j \geq 0, \quad j\epsilon D_0 \\ \underline{x}_j \leq x_j, \quad j\epsilon D_1 \\ x_j \leq \bar{x_j}, \quad j\epsilon D_2 \\ \underline{x}_j \leq x_j \leq \bar{x_j}, \quad j\epsilon D_3 \end{array} \right\} \tag{23}$$

$L = D_0 \bigcup D_1 \bigcup D_2 \bigcup D_3$

Where $\underline{x}_j$ and $\bar{x_j}$ are additional constraints from below and above on the mole amount of jth dependent components respectively. These constraints are used when the quantity of some dependent components are known in advance.

v_j, the partial derivatives of $G(x)$ by x_j are:

$$v_j = \frac{\partial G(x)}{\partial x_j} \tag{24}$$

$$= C_j + ln(x_j/X_k), \qquad j\epsilon L|S_w, \qquad k\epsilon\phi \tag{25}$$

$$= C_j + ln(x_j/X_w) - ln(x_{jw}/X_w) - x_{jw}/X_w + 1, \qquad j\epsilon S_w^0 \tag{26}$$

where:

$$X_w = \sum_j x_j, \qquad j\epsilon S_w \tag{27}$$

Assuming that total Gibbs free energy of the system, $G(x)$, and its bounded set of constraints, $M1$, are both convex, the solution of the total Gibbs free energy minimization problem is as follows:

$$\mathbf{v} - \mathbf{A}^T\hat{\mathbf{u}} \geq 0, \tag{28}$$

$$\mathbf{A}\hat{\mathbf{x}} = \mathbf{b}, \qquad \hat{\mathbf{x}} \geq 0 \tag{29}$$

$$\hat{\mathbf{x}}^T(\mathbf{v} - \mathbf{A}^T\hat{\mathbf{u}}) = 0. \tag{30}$$

In these equations, which are Karush-Kuhn-Tucker (KKT) necessary and sufficient conditions of equilibrium, v_j and u_i are the normalized chemical potential of dependent components and the normalized chemical potential of independent components respectively. $\hat{}$ operator shows the optimal state of the variable and ^{T} is the vector

transpose operator.

From equations 15 and 28:

$$g_j/RT + lnc_j + ln\gamma_j + const - \sum_i a_{ij}\hat{u}_i \geq 0, \qquad j\epsilon L, i\epsilon N \tag{31}$$

Equation 30 ensures that the mole amounts of unstable species and phases are zero. Limiting the indices to L_s prevents the appearance of partial derivatives v_j equal to $-\infty$.

$$L_s = \{j | j\epsilon l_k, k\epsilon\phi, n(l_k) = 0 \vee n(l_k) = 1 \vee n(l_k) > 0 \wedge x_j > \varepsilon\} \tag{32}$$

Where $\varepsilon > 0$ is an operational threshold (usually between 10^{-40} and 10^{-20} mol). Species whose amounts are smaller than ε are removed from phase assemblage.

Table 8: Properties of the Sample Model

Property	**Amount**	**Unit**
Temperature	348.15	Kelvin
Pressure	100	Kpa
Volume V of reactive subsystem	64.4378	m^3
Mass of reactive subsystem	119.7	Kg
pH of aqueous solution in molal activity scale	19.3816	

3.2.2 A Numerical Model Example

In this section, the details of a model calculated by GEM Selektor 3.0 will be laid out. For this purpose, thermodynamic model of the control geopolymer with fly ash type F cured at 75 degrees Celsius was used. The initial input data and bulk composition is shown in tables 8 and 9.

The bulk composition of reactive subsystem matrix (**b**) is determined by Gems as follows:

$$\left\{\begin{array}{cccccccccc} \text{Al} & \text{Ca} & \text{Fe} & \text{H} & \text{K} & \text{Mg} & \text{Na} & \text{Nit} & \text{O} & \text{Si} \\ 232.64 & 14.27 & 36.20 & 1963.69 & 7.01 & 15.38 & 283.70 & 3569.72 & 2449.51 & 444.71 \\ \text{Kg} & \text{Kg} & \text{Kg} & \text{Kg} & \text{Kg} & \text{Kg} & \text{Kg} & \text{Kg} & \text{Kg} & \text{Kg} \end{array}\right\} \tag{33}$$

Table 9: Bulk Composition of Independent Components for the Sample Model

Name	Al_2O_3	H_2O	CaO	Fe_2O_3	K_2O	MgO	Na_2O	NaOH	SiO_2	Nit
Quantity	11.86	16.9	0.8	2.89	0.33	0.62	6.08	3.5	26.72	50000
Units	Kg	Kg	Kg	Kg	Kg	Kg	Kg	Kg	Kg	g

The dimensionless chemical potential of independent components matrix (**u**) is also determined:

Al	Ca	Fe	H	K	Mg	Na	Nit	O	Si
-280.92	-235.32	29.19	-39.69	-116.32	-200.22	-105.61	-1.79	-4.55	-286.72

(34)

Activity coefficients of dependent components ($\gamma_{j,k}$) in their respective phases, used in equation (14) in the previous chapter, are calculated by Gems. Here, a truncated matrix is presented to save space. A total of 77 dependent components are included in the matrix.

Ca^{2+}	Fe^{2+}	K^{+}	Mg^{2+}	Na^{+}	SiO_2@	SiO_3^{2-}
1.87e+020	1.87e+020	109076.41	1.87e+020	109076.41	0.91	1.87e+020

(35)

The stoichiometry matrix (**A1**) for dependent components is a matrix with rows equal to the number of dependent components and columns equal to the number of independent components (nDC*nIC).

$$
\left\{
\begin{array}{cccccccccccc}
0 & 1 & 0 & 0 & 0 & 0 & 0 & 0 & 0 & 0 & 2 \\
0 & 0 & 1 & 0 & 0 & 0 & 0 & 0 & 0 & 0 & 2 \\
0 & 0 & 0 & 0 & 1 & 0 & 0 & 0 & 0 & 0 & 1 \\
0 & 0 & 0 & 0 & 0 & 1 & 0 & 0 & 0 & 0 & 2 \\
0 & 0 & 0 & 0 & 0 & 0 & 1 & 0 & 0 & 0 & 1 \\
0 & 0 & 0 & 0 & 0 & 0 & 0 & 0 & 2 & 1 & 0 \\
0 & 0 & 0 & 0 & 0 & 0 & 0 & 0 & 3 & 1 & -2 \\
0 & 0 & 0 & 1 & 0 & 0 & 0 & 0 & 1 & 0 & -1 \\
0 & 0 & 0 & 1 & 0 & 0 & 0 & 0 & 0 & 0 & 1 \\
0 & 0 & 0 & 2 & 0 & 0 & 0 & 0 & 1 & 0 & 0 \\
0 & 0 & 0 & 2 & 0 & 0 & 0 & 0 & 0 & 0 & 0 \\
0 & 0 & 0 & 0 & 0 & 0 & 0 & 2 & 0 & 0 & 0 \\
0 & 0 & 0 & 0 & 0 & 0 & 0 & 0 & 2 & 0 & 0 \\
0 & 0 & 0 & 2 & 0 & 0 & 0 & 0 & 1 & 0 & 0 \\
0 & 1.666667 & 0 & 4.2 & 0 & 0 & 0 & 0 & 5.766667 & 1 & 0 \\
0 & 0.833333 & 0 & 2.666666 & 0 & 0 & 0 & 0 & 4.166666 & 1 & 0 \\
0 & 1.5 & 0 & 5 & 0 & 0 & 0 & 0 & 6 & 1 & 0 \\
0 & 1.25 & 0 & 5 & 0 & 0 & 0 & 0 & 6.25 & 1.25 & 0 \\
0 & 1 & 0 & 5 & 0 & 0 & 0 & 0 & 6.5 & 1.5 & 0 \\
0 & 0.8333 & 0 & 3.6666 & 0 & 0 & 0 & 0 & 4.6666 & 1 & 0 \\
0 & 0 & 0 & 0.9 & 0.5 & 0 & 0 & 0 & 1.1 & 0.2 & 0 \\
\ldots
\end{array}
\right\} \quad (36)
$$

By solving Karush-Kuhn-Tucker (KKT) necessary and sufficient conditions of equilibrium (equations 28 to 30), the $\hat{\mathbf{x}}$ matrix, withprimal optimal solution of the problem with dependent components mole amounts is determined. The results are calculated in terms of percentage in the geopolymer mass.

3.3 Flowchart

The methodology phases described in the previous sections are depicted in the flowchart below (Figure 7). As it is emphasized, the data from the previous phases are used to realize the goal of the next phase. The data from the prescreening tests in the experimental phase shows which mix designs where disintegrated and should be followed up to understand which species caused the failure. Also, all failed samples are compared to each other to find a common cause of failure. Input data of the mix designs are going to be used in thermodynamic modeling and the resulting phases are going to be calculated. In the end, the output results from the models are compared to the leaching test results.

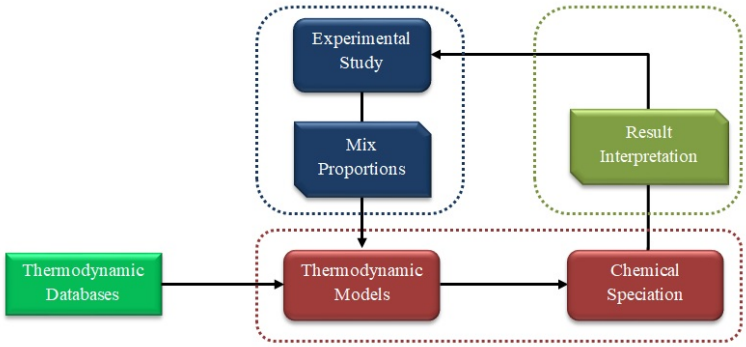

Figure 7: Research plan flowchart

CHAPTER 4: RESULTS AND DISCUSSION

4.1 Phase One: Experimental Phase

4.1.1 Leachability test

As the geopolymer matrix was proposed for physical sequestration of the waste, the monolith should remain intact throughout the leaching test process. Therefore, method 1315 or tank test was considered for the leaching study [22]. This method is used to assess the leaching and immobilization of halides from geopolymer mix designs. For this purpose, the monoliths were immersed in tanks containing deionized water and the leachate was collected at certain time intervals in days (0.08d, 1d, 2d, 7d, 14d, 28d, 42d, 49d and 63d). The liquid-surface-area ratio (L/A) must be maintained at $9 \pm 1 \quad mL/cm^2$. The leachate pH, ORP, conductivity and ion concentration was measured for each interval.

Table 10 shows the minimum detection limit for the target analytes. Based on this table and results from the ion concentration analysis using ion chromatography, phosphate and fluoride were at minimum detection limit for all the recipes.

The dominant release mechanism of the analytes at different time intervals can

Table 10: Minimum detection limit for target analytes

Anions	Minimum Detection Limit (ppm)	Ion Chromatography Results (ppm)
Fluoride	0.125	<0.125
Chloride	0.3125	86000
Bromide	0.125	2700
Nitrate	0.125	77
Phosphate	0.125	<0.10
Sulfate	1.25	3730

be predicted using this arbitrary guiding line. Based on the slope value, the three dominant release mechanisms are as follows: < 0.35 represents leaching due to surface wash-off or depletion. 0.35 to 0.65 represents leaching due to diffusion from the monoliths and 0.65 represents leaching due to dissolution from the monoliths.

Studying the graphs shows that the dominant release mechanism in the control sample is due to dissolution from the monolith whereas in case of the other monoliths, leaching is due to surface wash-off or depletion. In the following sections, these mechanisms are discussed in detail for different analytes.

Chloride: Chloride was detected in leachates from all different intervals. The leaching mechanism from the mix designs was mainly surface depletion. However, the rate was reduced at the end of leaching period. The control sample showed dissolution leaching behavior(Figure 8).

Figure 9 shows the average leaching percentage from different mixes. Mix design S6.5-C30 showed the best sequestration success.

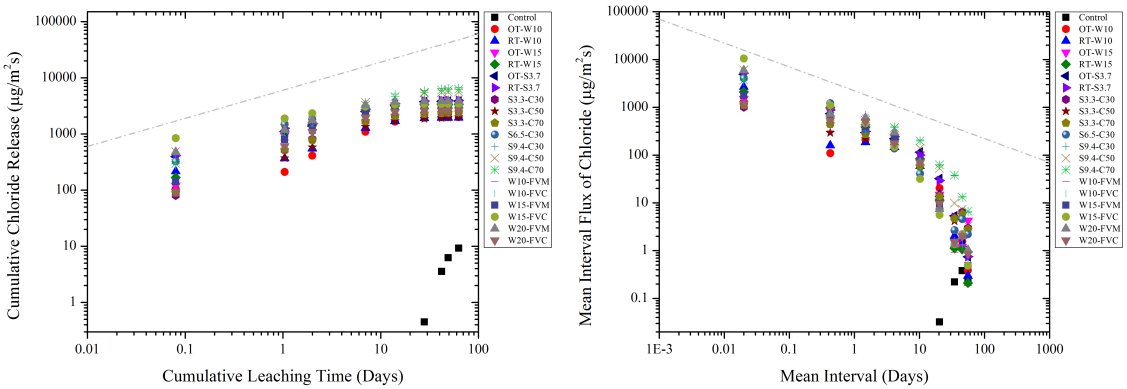

Figure 8: Cumulative Chloride Release and Mean Interval Flux of Chloride

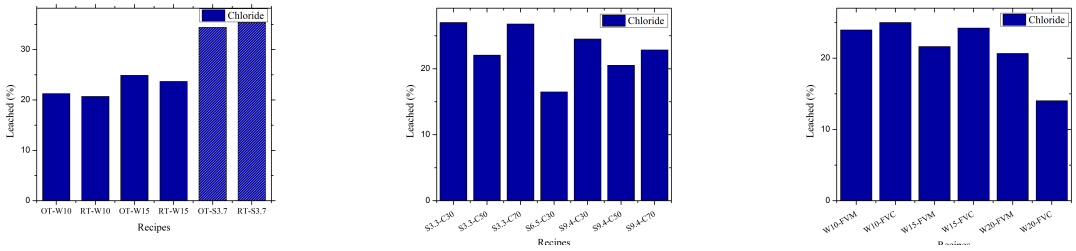

Figure 9: Chloride Average Leaching Percentage

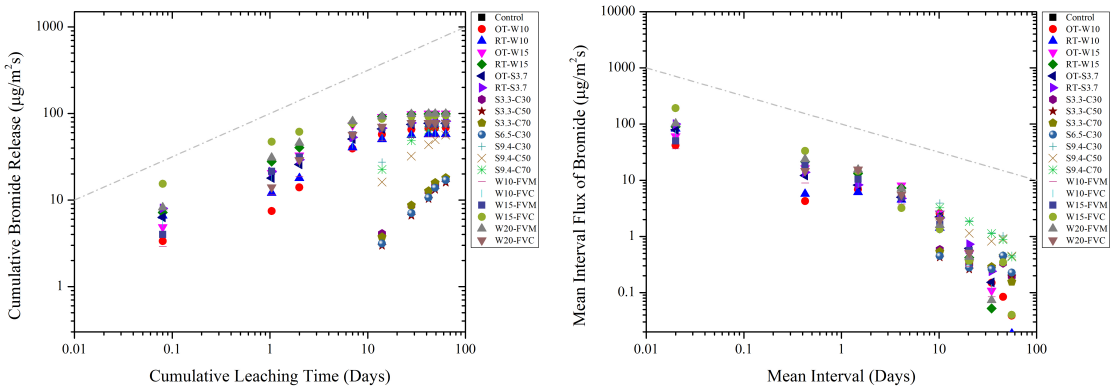

Figure 10: Cumulative Bromide Release and Mean Interval Flux of Bromide

Bromide: In samples made with FGD wastewater, bromide showed diffusion leaching behavior at the early stages. The leaching rate was reduced at the end of leaching period. The samples made with dry ZLD salt and compaction showed a completely different behavior. In these samples, the dominant release mechanism was dissolution and diffusion. No leaching observed from control samples (Figure 10)

The average leaching percentage of bromide from mix designs (Figure 11) also indicate that samples made with dry salt and compaction had higher efficiency to decrease the leaching of bromide from monoliths.

Nitrate: The dominant release mechanism for samples made with dry salt and compaction was dissolution. The control samples showed similar behavior. The other samples showed surface depletion release mechanism (Figure 12).

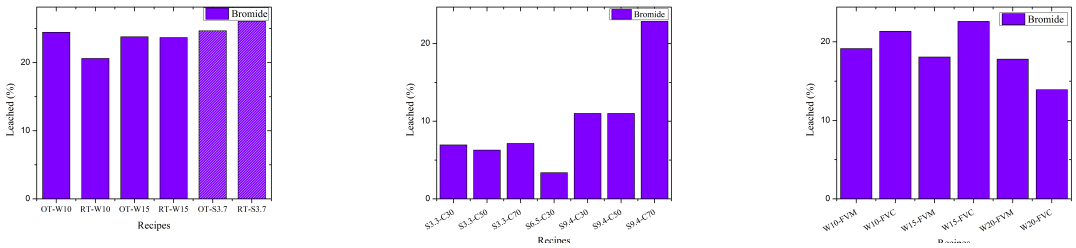

Figure 11: Bromide Average Leaching Percentage

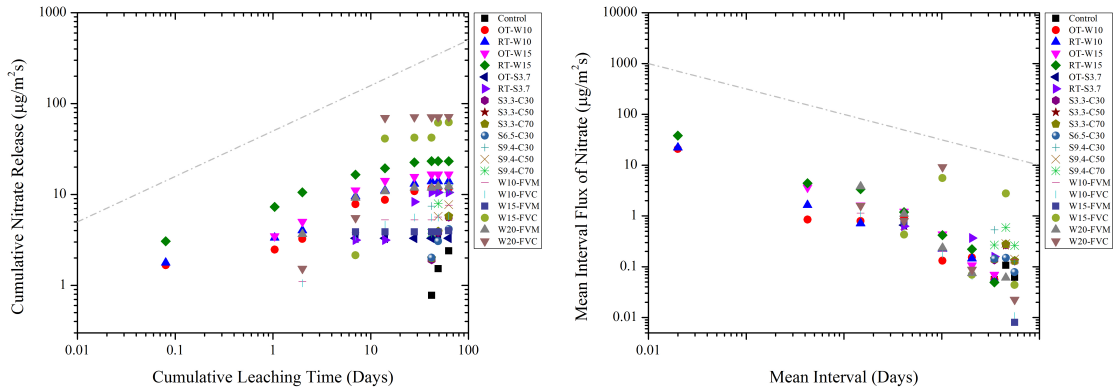

Figure 12: Cumulative Nitrate Release and Mean Interval Flux of Nitrate

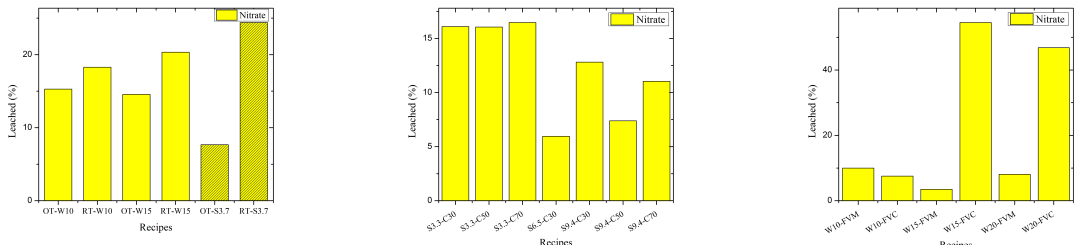

Figure 13: Nitrate Average Leaching Percentage

Low leaching percentage of samples made with dry ZLD salt is evident in case of nitrate. Mix design S6.5-C30 specifically showed the best sequestration efficiency with only 0.07 percent leached (Figure 13).

Sulfate: The release mechanism of sulfate was mainly surface depletion. However, samples made with dry salt showed dissolution and diffusion leaching behavior at early stages. It is believed that the monolith dissolution has contributed to high amounts of sulfate in the samples (Figures 14). High amounts of sulfate leaching in

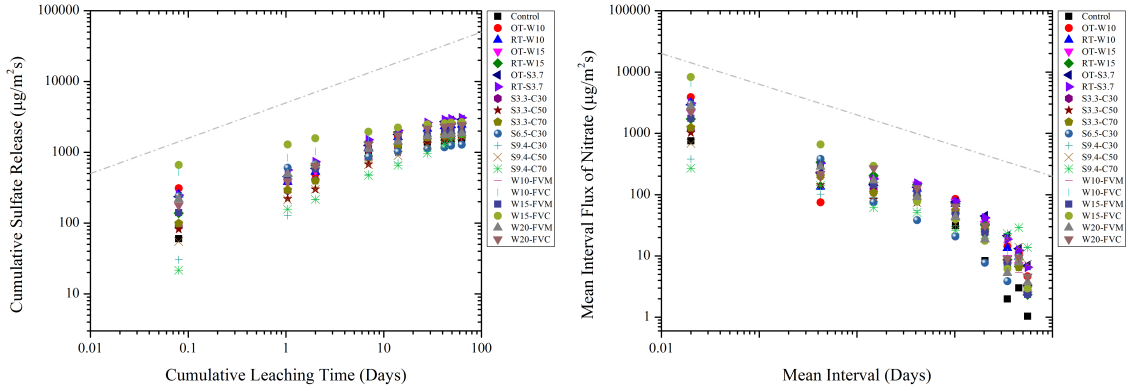

Figure 14: Cumulative Sulfate Release and Mean Interval Flux of Sulfate

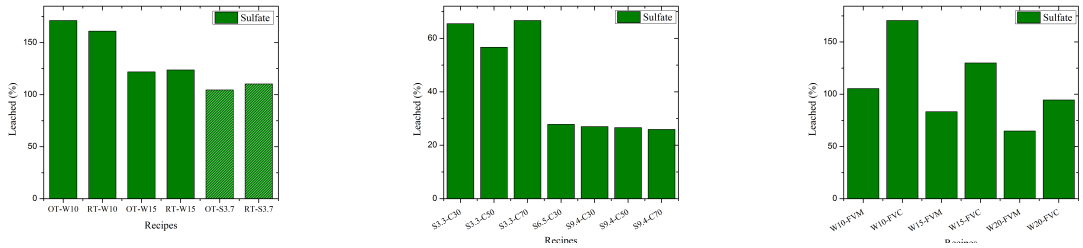

Figure 15: Sulfate Average Leaching Percentage

all the samples could be due to the dissolution of fly ash particles during geopolymerization process and release of this analyte to the pore space of the monolith. Dry salt samples show better sequestration compared to FGD wastewater samples (Figure 15). Table 11 shows mass release of anions from the control samples. It can be seen that the geopolymerization process has increased leaching anions, especially nitrate and sulfate, from the matrix. Through dissolution of fly ash particles in the highly alkaline activator, these anions are released.

The leaching percentages of the other samples were calculated without considering this issue. However, the leaching percentages for chloride, bromide and nitrate show relatively good sequestration. As seen in the graphs, although the geopolymer matrix releases some amounts of chloride and nitrate, the chloride and nitrate percentage released does not exceed 36 and 55 percent respectively. The leaching percentages of sulfate are extraordinarily high in some cases which is thought to be due to release from the geopolymer matrix.

Table 11: Average concentration of anions in the geopolymer recipes

	AVERAGE CONCENTRATION			
	Chloride	Bromide	Nitrate	Sulfate
	mg/Kg	mg/Kg	mg/Kg	mg/Kg
Control	1.66	0.07	0.22	823.89
W10	9408.96	280.07	76.15	1525.29
W15	14112.60	420.06	114.14	2054.87
S3.7 *	11208.02	312.35	43.07	2784.81
S3.3 *	9088.01	253.27	35.01	2718.81
S6.5 *	18174.37	506.47	69.81	4613.73
S9.4 *	27260.72	759.66	104.60	6508.65
W10-FVM	9409.07	280.07	76.21	1883.13
W10-FVC	9408.96	280.07	76.15	1525.29
W15-FVM	14112.70	420.06	114.19	2376.92
W15-FVC	14112.60	420.06	114.14	2054.87
W20-FVM	18816.33	560.06	152.18	2870.72
W20-FVC	18816.24	560.06	152.13	2572.52

4.1.2 Geopolymer Sequestration Efficiency

In order to have a better understanding of the sequestration efficiency of the prepared recipes, an arbitrary criterion was introduced. In this efficiency criterion, different variables including mass sequestered, time, cost and equipment are calculated. Based on the direct or inverse relationship of the variables, they were placed in the numerator or denominator. Also, a weighted scale was introduced depending on the importance of the variable. The lowest number in the last column would represent the best option for sequestration (Table 12).

The first column shows the mix design names. In the second column, mass in

grams, represents the cylinder mass. Mass sequestered is the mg amount of salt sequestered in a Kg of sample. In the next column, the second column of the table is divided by the third column and multiplied by 10^6. The amount of time needed to prepare the samples is taken into account in the fifth column. If the samples were cured in the oven, 5 points were considered in the sixth column. The cost of the sample, based on the approximate price of the ingredients is presented in column seven. This amount is multiplied by 5 as an arbitrary factor in the eighth column. The samples were ranked from 1 to 5 based on the equipment requirement in the ninth column. The tenth column takes an arbitrary 2 multiplier to the equipment column. The efficiency score is calculated in the eleventh column. The lowest score is considered to have the highest rank of efficiency.

The results show that the mix with 9.4 percent of dry salt and 50 proctor hammer compaction (equivalent to 50618 ft.lb/ft3 of energy) is the best choice. Also, the graphs presented in the previous section show that the leaching percentages from the mentioned samples are low.

Table 12: Sequestration efficiency criterion

	Mass (g)	Mass Sequestered (mg/Kg)	Mass GP/ZLD Sequestered ($x10^6$)	Time (Hours)	Energy	Cost	x5	Equipment (1-5)	x2	Efficiency	Rank
OT-W10	1179.43	11290.47	104462.5	24	5	293.3	1466.5	2	4	69.66	
RT-W10	1237.20	11290.47	109578.7	24	0	293.3	1466.5	1	2	73.42	
OT-W15	1075.95	16701.67	64421.4	24	5	288.7	1443.5	2	4	43.63	
RT-W15	1160.1	16701.67	69460.11	24	0	288.7	1443.5	1	2	47.27	
OT-S3.7	1282.16	14348.25	89360.06	24	5	293.3	1466.5	2	4	59.59	
RT-S3.7	1297.07	14348.25	90398.86	24	0	293.3	1466.5	1	2	60.57	
S3.3-C30	1029.07	12095.1	85081.54	24	5	288.9	1444.5	3	6	57.51	
S3.3-C50	986.19	12095.1	81535.89	24	5	288.9	1444.5	3	6	55.11	
S3.3-C70	1030.76	12095.1	85221.27	24	5	288.9	1444.5	3	6	57.60	
S6.5-C30	977.5	23364.37	41837.22	24	5	287.3	1436.5	3	6	28.43	5
S9.4-C30	1066.01	34633.63	30779.62	24	5	285.7	1428.5	3	6	21.03	2
S9.4-C50	1046.80	34633.63	30224.81	24	5	285.7	1428.5	3	6	20.65	1
S9.4-C70	1084.4	34633.63	31310.61	24	5	285.7	1428.5	3	6	21.39	3
W10-FVM	1089.57	11648.47	93537.64	48	5	287.3	1436.5	5	10	62.38	
W10-FVC	1127.41	11290.47	99854.61	48	5	293.3	1466.5	5	10	65.29	
W15-FVM	1003.51	17023.87	58946.93	48	5	283.3	1416.5	5	10	39.84	7
W15-FVC	1003.87	16701.67	60105.96	48	5	288.7	1443.5	5	10	39.90	8
W20-FVM	917	22399.28	40938.82	48	5	279.3	1396.5	5	10	28.05	4
W20-FVC	1074.97	22100.94	48638.87	48	5	284.3	1421.5	5	10	32.76	6

4.2 Phase Two: Modeling

A thermodynamic database was adopted using the natural zeolites database [73] together with the cement database (CEMDATA 2018) developed by EMPI [58]. From the natural zeolites database, species occurring in low temperature skarns, hydrothermal environments and saline-alkaline lake environments were selected [7]. Different mix designs containing varying percentages of either solid zero discharge liquid (ZLD) salt or flue gas desulfurization (FGD) wastewater cured at 75 degrees Celsius and room temperature were modeled using GEM Selektor 3 [50]. Also, a model developed for the solid solution of activator together with FGD wastewater at room temperature to understand the cause of coagulation of the solution. Models developed under different conditions showed that there was not a difference in the resulting solid chemistry after the use of compaction or vacuum. Moreover, the time the system needs to reach equilibrium was not taken into consideration in the models and it was assumed all the samples had already reached equilibrium. In other words, kinetics were not considered in the models.

In order to understand the baseline for geopolymer phase assemblage, four geopolymer designs were modeled;types F and F-C geopolymers, cured at 75 degrees Celsius and the same mix designs cured at room temperature. The mix breakdown of these geopolymers is shown in table 13.

Table 13: Mix Breakdown of Control Samples

	Curing Temp.	Fly Ash F	Fly Ash C	NaOH	Sodium Silicate (Type O)	H_2O
Control-F-OT	75	41.40	0.00	3.50	10.60	16.90
Control-F-RT	25	41.40	0.00	3.50	10.60	16.90
Control-FC-OT	75	24.00	21.00	2.90	8.50	13.60
Control-FC-RT	25	24.00	21.00	2.90	8.50	13.60

Table 14: Chemical Constituents of Control Samples

	Al_2O_3	$Aqua$	CaO	Fe_2O_3	K_2O	MgO	Na_2O	$NaOH$	SiO_2
Unit	Kg	Kg	Kg	Kg	Kg	Kg	Kg	Kg	Kg
Control-F	11.86	16.90	0.80	2.89	0.33	0.62	6.08	3.50	26.72
Control-FC	10.92	13.60	5.35	2.98	0.36	0.67	5.08	2.90	24.91

Based on the breakdown in the table and the amounts of components in each sample, the detailed chemical constituents of each mix was calculated (Table 14). The data from this table was used as input for GEM Selektor model.

The main component of geopolymer samples developed with class F fly ash is natrolite ($Na_2Al_2Si_3O_{10}.2H_2O$) [46, 68, 76, 3]. It is a fibrous zeolite [7] with brittle tenacity and hardness of 5-5.5 [2]. This zeolite shows fiber-like morphology [34]. The second most abundant zeolite in geopolymer samples treated in the oven is analcime ($NaAlSi_2O_6.H_2O$) [45, 25]; a single connected 4-ring chain zeolite [34] with brittle tenacity and hardness of 5-5.5 [2]. This zeolite is responsible for the high density and imperviousness of class F geopolymer cured in the oven. This zeolite was not formed in other control samples (Figure 16).

On the other hand, the main component of geopolymer samples developed with

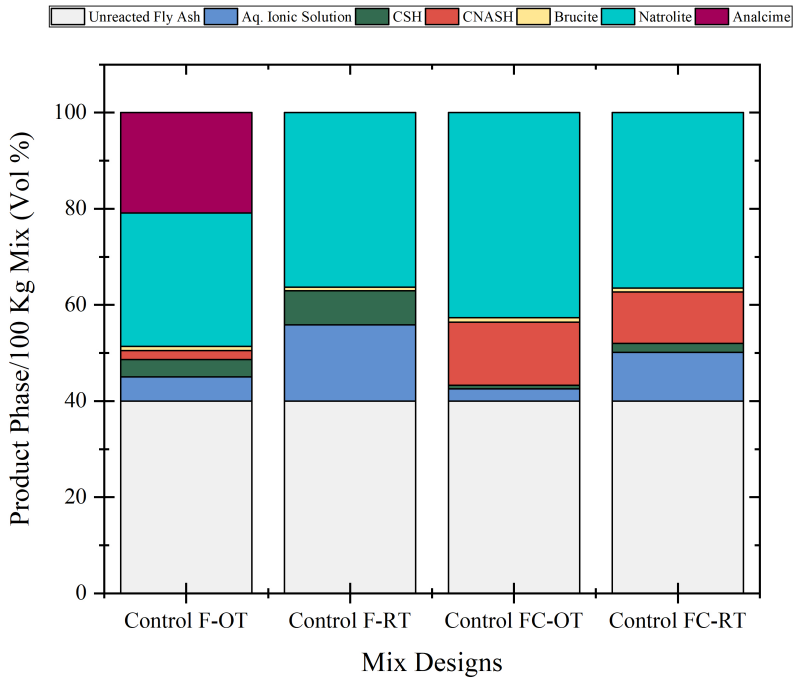

Figure 16: Control samples phase assemblage

both class F and class C fly ash is natrolite ($Na_2Al_2Si_3O_{10}.2H_2O$). Analcime did not form in these geopolymer samples. However, due to higher Ca content, calcium silicate hydrate ($C-S-H$) [49, 31] and calcium (alkali) aluminosilicate hydrate ($C-(N-)A-S-H$) [64, 63, 86] phases are formed. $C-S-H$ is the main component formed in ordinary portland cement binder.

An aqueous ionic pore solution constitutes a portion of control samples. This portion, is lower in Control-FC samples (2.56 and 10.12 Vol%) while it reaches 5.03 to 15.86 Vol% for Control-F-OT and Control-F-RT respectively. Generally, the volume

of ionic pore solution is higher in samples cured at room temperature which is the primary reason for lower compressive strength in these samples.

With the addition of ZLD salt or FGD wastewater, the phase assemblage of the geopolymer samples completely change. Therefore, the cases are studied separately first and common findings will be compared across different groups of mixes. The design of different mixes and their curing conditions are presented in table 15. In these mix designs, the amount of water present in sodium silicate is counted towards the overall water content in each sample. Also, 40% of the fly ash content was assumed to stay as unreacted fly ash. The curing temperature is in degrees C and the unit for all components is Wt%. In the following sections, the phase assemblages of each mix group and their stabilities are compared with each other.

Table 15: Mix Breakdown of Samples Prepared with Solid ZLD Salt and FGD Wastewater

Mix Name	Curing Temp.	Solid FGD	Fly Ash F	Fly Ash C	NaOH	Sodium Silicate (Type O)	H2O
S3.3	75	3.30	40.20	0.00	3.40	10.20	16.10
S3.7	75	3.70	39.00	0.00	3.40	10.60	17.30
S6.5	75	6.50	39.00	0.00	3.30	9.70	15.50
S9.4	75	9.40	37.80	0.00	3.20	9.40	15.00

Mix Name	Curing Temp.	FGD Wastewater (Brine)	Fly Ash F	Fly Ash C	NaOH	Sodium Silicate (Type O)	H2O
WW10-F-OT	75	10.00	39.00	0.00	2.90	8.50	13.60
WW15-F-OT	75	15.00	36.00	0.00	2.90	8.50	13.60
WW20-F-OT	75	20.00	33.00	0.00	2.90	8.50	13.60
WW25-F-OT	75	25.00	30.00	0.00	2.90	8.50	13.60
WW30-F-OT	75	30.00	27.00	0.00	2.90	8.50	13.60
WW10-F-RT	25	10.00	39.00	0.00	2.90	8.50	13.60
WW15-F-RT	25	15.00	36.00	0.00	2.90	8.50	13.60
WW20-F-RT	25	20.00	33.00	0.00	2.90	8.50	13.60
WW25-F-RT	25	25.00	30.00	0.00	2.90	8.50	13.60
WW30-F-RT	25	30.00	27.00	0.00	2.90	8.50	13.60
WW10-FC-OT	75	10.00	21.00	18.00	2.90	8.50	13.60
WW15-FC-OT	75	15.00	19.80	16.20	2.90	8.50	13.60
WW20-FC-OT	75	20.00	18.00	15.00	2.90	8.50	13.60
WW25-FC-OT	75	25.00	16.20	13.80	2.90	8.50	13.60
WW30-FC-OT	75	30.00	15.00	12.00	2.90	8.50	13.60
WW10-FC-RT	25	10.00	21.00	18.00	2.90	8.50	13.60
WW15-FC-RT	25	15.00	19.80	16.20	2.90	8.50	13.60
WW20-FC-RT	25	20.00	18.00	15.00	2.90	8.50	13.60
WW25-FC-RT	25	25.00	16.20	13.80	2.90	8.50	13.60
WW30-FC-RT	25	30.00	15.00	12.00	2.90	8.50	13.60

4.2.1 Thermodynamic Model of Type F Geopolymers Containing Solid ZLD Salt (S Series)

As it was shown in the previous section, this series of geopolymers were developed with varying percentages of solid ZLD salt and class F geopolymer gel. The mix breakdown of this series which was used as the input for the thermodynamic models is presented in table 16.

The main component of geopolymers in this group is analcime ($NaAlSi_2O_6.H_2O$) [45, 25] at lower salt contents which is replaced by higher volumes of amorphous silica when the amount of salt increases. Analcime is the only zeolite phase that is formed in the geopolymer. With increase in salt content, due to the availability of SO_4^{2-} ion from the salt, alunite $KAl_3(SO_4)_2(OH)_6$, anhydrite $CaSO_4$ and thenardite Na_2SO_4 species develop and increase. All these three species have brittle tenacity with hardness of 3.5-4, 3-3.5 and 2.5-3, respectively [2]. Thenardite which specifically increases with the increase of salt content in the geopolymers is soluble in water and this seems to be the reason behind the instability of the samples in aqueous environment after

Table 16: Chemical Constituents of Geopolymer Samples Prepared with ZLD Solid Salt

	Al_2O_3	$Aqua$	CaO	Fe_2O_3	K_2O	MgO	Na_2O	$NaOH$	SiO_2	Br^-	Cl^-	NO_3^-	SO_4^{2-}
Unit	Kg	Kg	Kg	Kg	Kg	Kg	Kg	Kg	Kg	a(mg/Kg)	a(mg/Kg)	a(mg/Kg)	a(mg/Kg)
S3.3	11.52	16.10	0.78	2.81	0.32	0.60	5.86	3.40	25.90	303600.00	2732400.00	310200.00	6910200.00
S3.7	11.17	17.30	0.76	2.73	0.31	0.58	6.04	3.40	25.47	340400.00	3063600.00	347800.00	7747800.00
S6.5	11.17	15.50	0.76	2.73	0.31	0.58	5.58	3.30	25.03	598000.00	5382000.00	611000.00	13611000.00
S9.4	10.83	15.00	0.73	2.64	0.30	0.56	5.41	3.20	24.26	864800.00	7783200.00	883600.00	19683600.00

curing. Another water soluble specie that increases with increase in solid salt is halite ($NaCl$) which is brittle with a very low hardness (2-2.5)[2]. The formation of these phases due to higher levels of Cl^- and SO_4^{2-} have resulted in decrease in charge balancing ions (Na^+, K^+ and Ca^{2+}) that help in the formation of zeolites. Therefore, the silicate that was forming analcime was shifted to the formation of amorphous silica (Figure 17).

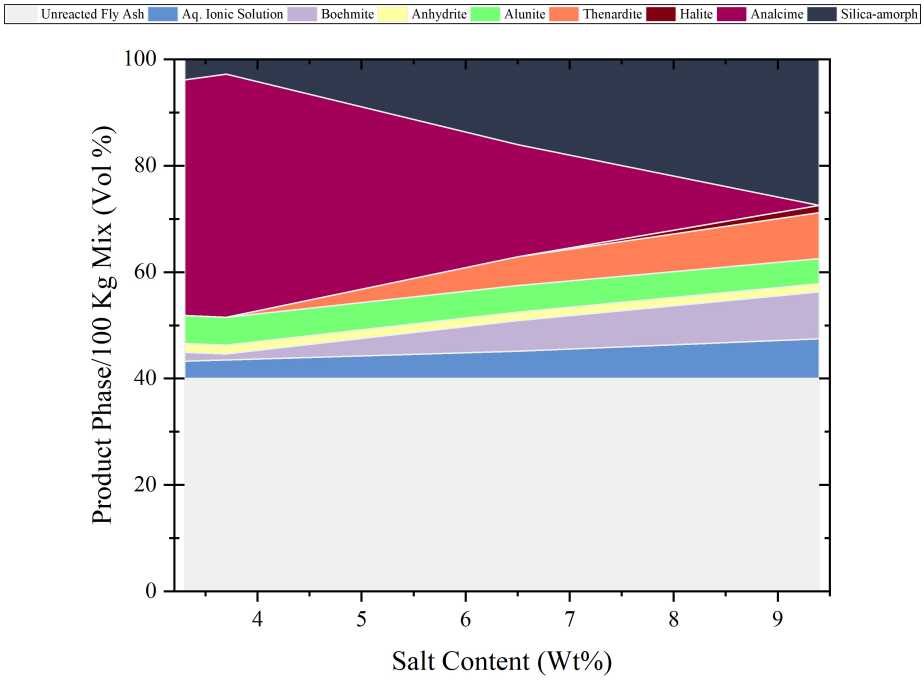

Figure 17: Solid ZLD Salt Samples (S Series) Phase Assemblage

Table 17: Chemical Constituents of Type F Geopolymers Containing FGD Wastewater

	Al_2O_3	$Aqua$	CaO	Fe_2O_3	K_2O	MgO	Na_2O	$NaOH$	SiO_2	Br^-	Cl^-	NO_3^-	SO_4^{2-}
Unit	Kg	Kg	Kg	Kg	Kg	Kg	Kg	Kg	Kg	a(mg/Kg)	a(mg/Kg)	a(mg/Kg)	a(mg/Kg)
WW10-F	11.17	22.51	0.76	2.73	0.31	0.58	4.98	2.90	24.44	28000.00	940750.00	7600.00	110700.00
WW15-F	10.31	26.97	0.70	2.52	0.29	0.54	4.93	2.90	22.88	42000.00	1411125.00	11400.00	166050.00
WW20-F	9.45	31.43	0.64	2.31	0.26	0.49	4.87	2.90	21.32	56000.00	1881500.00	15200.00	221400.00
WW25-F	8.60	35.88	0.58	2.10	0.24	0.45	4.82	2.90	19.77	70000.00	2351875.00	19000.00	276750.00
WW30-F	7.74	40.34	0.52	1.89	0.22	0.40	4.77	2.90	18.21	84000.00	2822250.00	22800.00	332100.00

4.2.2 Thermodynamic Model of Type F Geopolymers Containing FGD Wastewater (WW-F Series)

This series of geopolymers were prepared with 10 to 30 percent of FGD wastewater. Two pairs of samples were prepared for each mix design; one pair was cured at 75 degrees Celsius for 24 hours whereas the other pair was cured at room temperature (25 degrees Celsius). Table 17 shows the detailed chemical Constituents of this series used as input for the thermodynamic models.

4.2.2.1 WW-F samples cured at 75 degrees Celsius (WW-F-OT)

Table 18 shows the phase assemblage of WW-F geopolymer samples cured at 75 degrees Celsius. The main zeolite phases formed in this series of geopolymers are analcime ($NaAlSi_2O_6.H_2O$) and natrolite ($Na_2Al_2Si_3O_{10}.2H_2O$). The models show that in oven-treated samples the total zeolite content decreases from 45.69 to 22.9 Vol%. Other phases formed in lower volumes include Fe monocarbonate (C_3FH_6) [59],

Table 18: Phase Assemblage of Geopolymer Samples Prepared with FGD Wastewater Cured in the Oven

Wastewater Content	10	15	20	25	30
Unreacted Fly Ash	40.00	40.00	40.00	40.00	40.00
Aq. Ionic Solution	12.07	18.72	25.12	30.76	35.75
monosulph-AlFe	0.00	0.00	0.00	0.00	0.00
monosulph-FeAl	0.51	0.89	1.16	1.35	1.11
C3FH6	1.19	0.71	0.31	0.00	0.00
Brucite	0.54	0.47	0.38	0.32	0.24
Natrolite	12.20	8.50	5.22	2.50	0.17
Analcime	33.49	30.71	27.80	25.06	22.73
Total Zeolites	45.69	39.21	33.02	27.57	22.90

Brucite ($Mg(OH)_2$) [66, 41] and Al-Fe-Monosulphate ($Ca_4(Al, Fe)_2(OH)_{12}.SO_4.6H_2O$) [19] (Figure 18). The pore solution with high amounts of anions increases dramatically with increase in FGD wastewater content. Low volumes of zeolites on one hand and high anion content and water in pore solution is the likely cause of disintegration in WW-F-OT samples with more than 20% FGD wastewater.

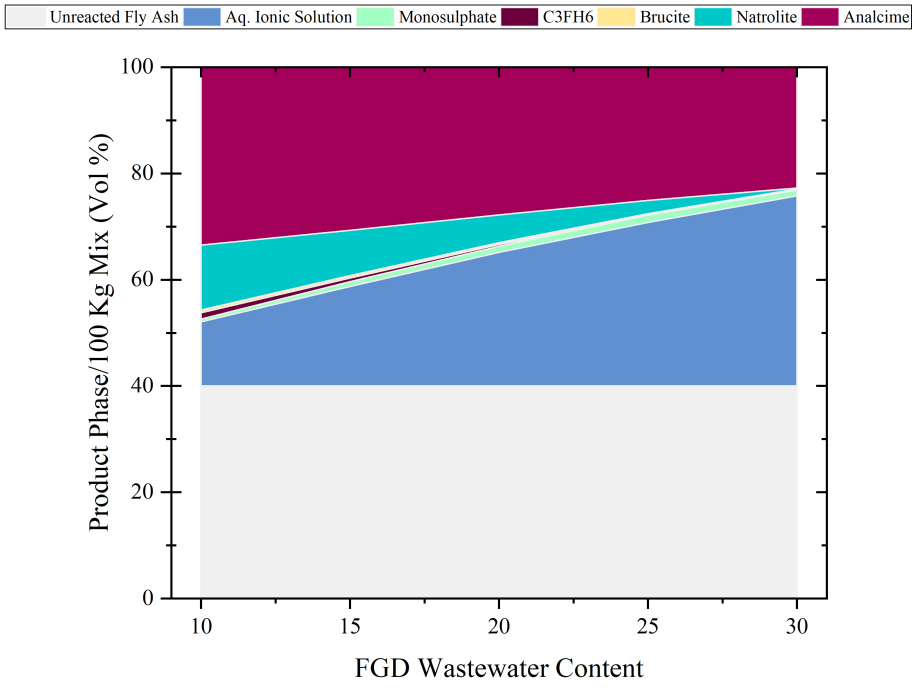

Figure 18: FGD Wastewater Type F Oven-treated Geopolymer Phase Assemblage

4.2.2.2 WW-F samples cured at room temperature (WW-F-RT)

The phase assemblage of WW-F-RT samples can be observed in table 19. The zeolite species formed in these samples are similar to the ones in oven-cured samples; analcime and natrolite. The total volume of these zeolites is evidently lower than that of the oven-treated geopolymers and ranges from 31.24 Vol%, in case of W10F-RT to 16.45 Vol%, when FGD wastewater content reaches 30%. In this group of mixes, ettringite ($Ca_6Al_2(SO_4)_3(OH)_{12}.26H_2O$) [2] was formed instead of Monosulphate phase. Although this expansive crystal is detrimental to concrete in the hardened state, its early formation does not harm the integrity of concrete. The volume of this phase increases with increase in the amount of FGD wastewater (Figure 19).

The volume of the ionic aqueous pore solution is much higher in mixes cured at

Table 19: Phase Assemblage of Geopolymer Samples Prepared with FGD Wastewater Cured at Room Temperature

Wastewater Content	10	15	20	25	30
Unreacted Fly Ash	40.00	40.00	40.00	40.00	40.00
Aq. Ionic Solution	27.26	32.01	36.04	39.46	42.45
ettringite-AlFe	0.00	0.00	0.00	0.00	0.00
ettringite-FeAl	0.38	0.54	0.67	0.79	0.89
C3FH6	0.83	0.59	0.38	0.21	0.06
Brucite	0.28	0.24	0.20	0.17	0.14
Natrolite	8.15	5.67	3.59	1.85	0.32
Analcime	23.09	20.95	19.12	17.52	16.14
Total Zeolites	31.24	26.62	22.71	19.37	16.45

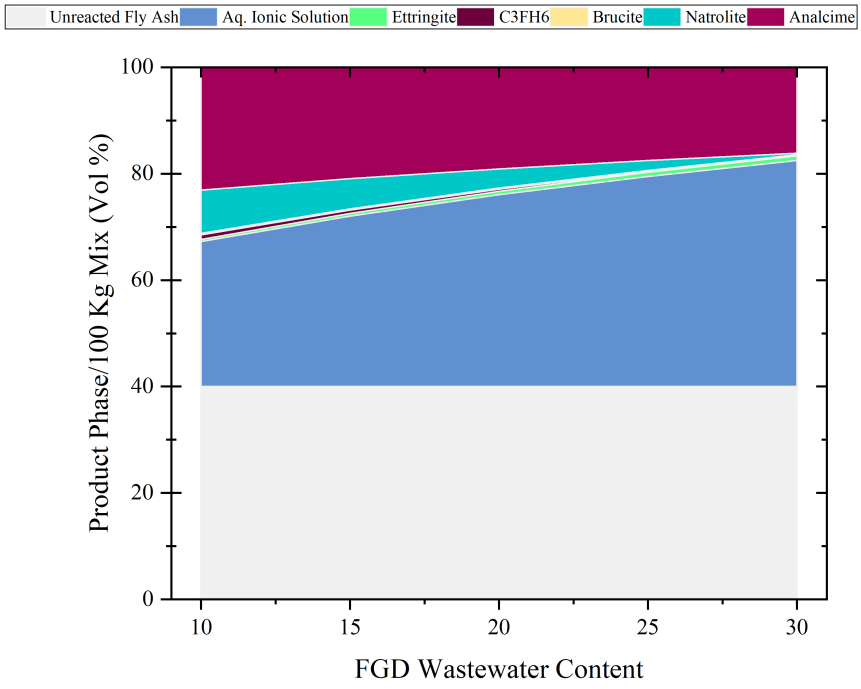

Figure 19: FGD Wastewater Type F Room-treated Geopolymer Phase Assemblage

room temperature compared to that of the mixes cured in the oven.

4.2.3 Thermodynamic Model of Type F and C Geopolymers Containing FGD Wastewater (WW-FC Series)

This series of samples were prepared using 10 to 30 percent of wastewater and they were cured at 75 degrees Celsius and room temperature. In these samples, fly ash type C, which contains higher amounts of calcium, was used instead of only fly ash type F. Table 20 shows the chemical constituents of these samples which were used as input for thermodynamic modeling. The phase assemblages of oven-treated and room-treated samples are studied in the following sections.

Table 20: Chemical Constituents of Type F and C Geopolymers Containing FGD Wastewater

	Al_2O_3	$Aqua$	CaO	Fe_2O_3	K_2O	MgO	Na_2O	$NaOH$	SiO_2	Br^-	Cl^-	NO_3^-	SO_4^{2-}
Unit	Kg	Kg	Kg	Kg	Kg	Kg	Kg	Kg	Kg	a(mg/Kg)	a(mg/Kg)	a(mg/Kg)	a(mg/Kg)
WW10-FC	9.48	22.51	4.59	2.59	0.31	0.58	4.98	2.90	22.17	28000.00	940750.00	7600.00	110700.00
WW15-FC	8.79	26.97	4.15	2.39	0.29	0.54	4.93	2.90	20.84	42000.00	1411125.00	11400.00	166050.00
WW20-FC	8.04	31.43	3.84	2.19	0.26	0.49	4.87	2.90	19.43	56000.00	1881500.00	15200.00	221400.00
WW25-FC	7.30	35.88	3.52	1.99	0.24	0.45	4.82	2.90	18.03	70000.00	2351875.00	19000.00	276750.00
WW30-FC	6.61	40.34	3.08	1.79	0.22	0.40	4.77	2.90	16.70	84000.00	2822250.00	22800.00	332100.00

Table 21: Phase Assemblage of Type F and C Geopolymer Samples Prepared with FGD Wastewater Cured at Oven Temperature

Wastewater Content	10	15	20	25	30
Unreacted Fly Ash	40.00	40.00	40.00	40.00	40.00
Aq. Ionic Solution	8.84	16.44	23.53	29.67	32.92
CSH	0.00	0.00	0.00	0.00	3.38
CNASH	5.51	4.57	3.86	3.20	3.06
C_3FH_6	5.65	4.76	3.99	3.32	1.77
arcanite	0.07	0.00	0.00	0.00	0.00
Brucite	0.81	0.70	0.57	0.48	0.40
Natrolite	22.79	16.99	12.34	8.13	4.01
Analcime	16.14	16.54	15.71	15.20	14.21
Total Zeolites	38.93	33.54	28.05	23.33	18.23

4.2.3.1 WW-FC samples cured at 75 degrees Celsius (WW-FC-OT)

Table 21 shows the amounts of phases formed in WW-FC-OT series. As it can be observed, the volume of zeolites (analcime ($NaAlSi_2O_6.H_2O$) and natrolite ($Na_2Al_2Si_3O_{10}.2H_2O$) is much lower than that of their counterparts in WW-F-OT series. The amount of analcime did not change with increase in wastewater content. However, natrolite volume decreased from 22.79 Vol% in WW10-FC-OT to 4.01 Vol% in WW30-FC-OT. Due to higher Ca2+ ion concentration in the gel, calcium silicate hydrate ($C-S-H$) [49, 31], calcium (alkali) aluminosilicate hydrate ($C-(N-)A-S-H$) [64, 86, 63] and Fe monocarbonate ($C3FH6$) [59] phases were also formed. These phases, together with a low zeolite volume helped these samples keep their integrity in the tank tests (Figure 20).

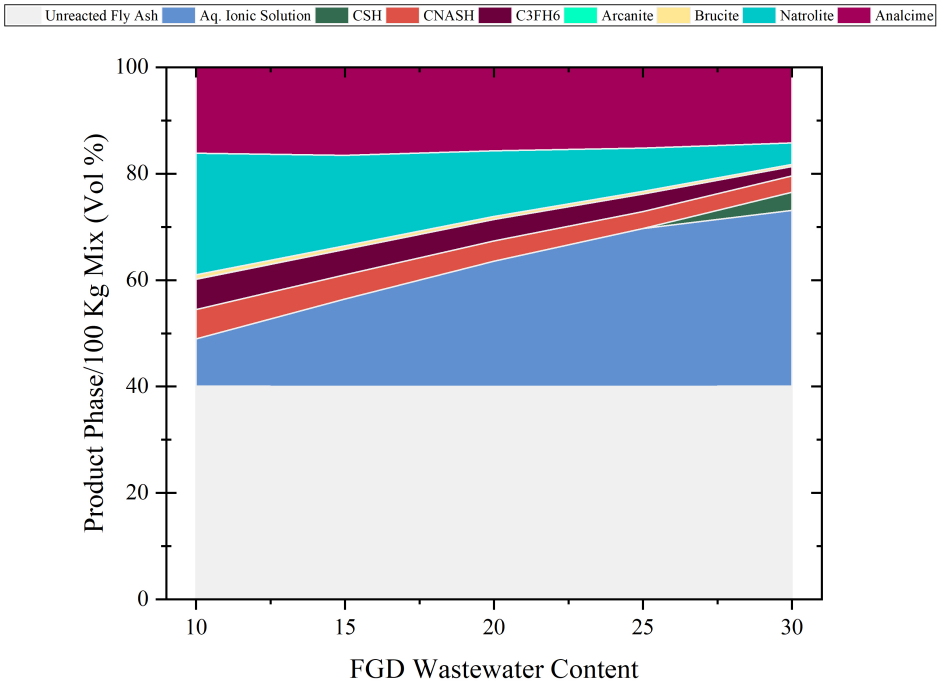

Figure 20: FGD Wastewater Type F and C Oven-treated Geopolymer Phase Assemblage

The aqueous ionic solution also increased from 8.84 Vol% in WW10-FC-OT to 32.92 Vol% in WW30-FC-OT which explains loss of compressive strength in these samples with increased wastewater content.

4.2.3.2 WW-FC samples cured at room temperature (WW-FC-RT)

The phase assemblage of WW-FC-RT series is demonstrated in table 22. In terms of zeolites formation, this series have lower zeolites compared to WW-FC-OT series which are cured in the oven. The only zeolite phase formed in these samples is low amounts of natrolite (24.71 Vol% in WW10-FC-RT to 12.34 Vol% in WW30-FC-RT). Cement hydration phases including calcium silicate hydrate ($C-S-H$), ettringite ($Ca_6Al_2(SO_4)_3(OH)_{12}.26H_2O$) and Fe monocarbonate ($C_3FH_6$) can be observed in small amounts too. The volume of these phases decreases with increase in wastewater content in the geopolymer. Despite lower volumes of zeolites and absence of analcime in this series, the presence of cement hydration phases improved the integrity of these geopolymer samples (Figure 21).

The volume of aqueous ionic pore solution also increases from 24.07 Vol% in WW10-FC-RT to 41.15 Vol% in WW30-FC-RT. This increase corresponds to loss of compressive strength of these samples with increase in the volume of FGD wastewater.

Table 22: Phase Assemblage of Type F and C Geopolymer Samples Prepared with FGD Wastewater Cured at Room Temperature

Wastewater Content	10	15	20	25	30
Unreacted Fly Ash	40.00	40.00	40.00	40.00	40.00
Aq. Ionic Solution	24.07	29.41	33.87	37.64	41.15
CSH	7.84	6.88	6.19	5.59	4.96
Ettringite	0.07	0.35	0.52	0.69	0.82
C_3FH_6	2.76	1.99	1.42	0.94	0.45
Brucite	0.56	0.47	0.39	0.33	0.26
Natrolite	24.71	20.91	17.60	14.81	12.34
Total Zeolites	24.71	20.91	17.60	14.81	12.34

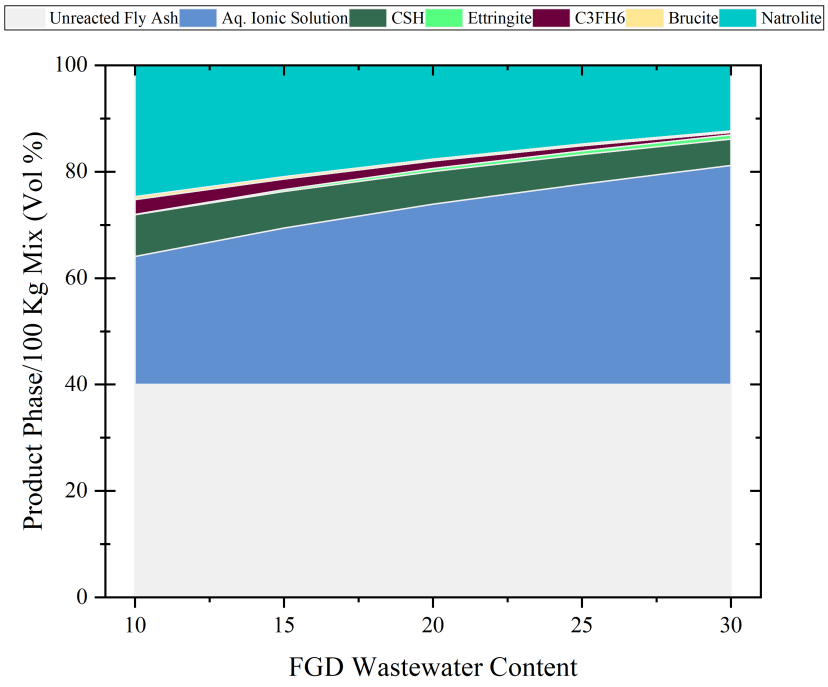

Figure 21: FGD Wastewater Type F and C Geopolymer treated at Room Temperature Phase Assemblage

CHAPTER 5: SUMMARY AND CONCLUSIONS

5.1 Research Summary

Type F fly ash (low calcium) and a mixture of type F and type C fly ash (high calcium) were used to create geopolymer samples containing flue gas desulfurization wastewater and zero liquid discharge salt (Figure 22). The percentages of type C and F fly ash were chosen experimentally based on the workability of the paste presented in chapter 3. The samples were cured at room temperature or in the oven for 24 hours. Based on these mix designs, chemical speciation models were developed.

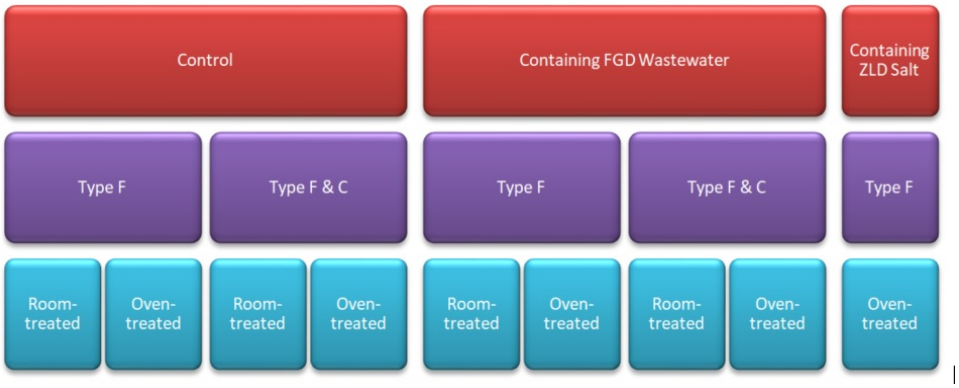

Figure 22: Different samples developed during the study

The study of geopolymer models and their comparison showed that the following are the main reasons behind the disintegration of alkali-activated fly ash contami-

nated with FGD wastewater:

- The formation of Cl^- and SO_4^2 salts result in decrease in charge balancing ions Na^+, K^+ and Ca^{2+} that would otherwise help in the formation of geopolymer matrix.

- The formation of low-strength species that caused discontinuation of geopolymer network.

- The formation of water-soluable species like Halite and Thenardite.

- Adding fly ash C to the mix improved the integrity of the material. This is due to the formation of species similar to the ones found in hydrated Portland cement.

5.2 Conclusions

The observations from chemical assemblage models developed in this study are consistent with the literature regarding the thermodynamic models of alkali-activated material as well as formation of natural zeolitic species.

The control samples containing fly ash type F (low calcium content) produced natrolite and analcime zeolites which are aluminous and silicic zeolites respectively. These crystalline phases potentially work as aggregates to improve the compressive strength of the alkali-activated material . This was shown in a study done by Phair

et. al. where addition of 3% zirconia crystals improved the compressive strength of the geopolymer[71]. The formation of natrolite was specifically observed in Myers models containing $\leq$ 41 Mass% CaO in alkali-activated blast furnace slag [66] (Figure 23). In naturally-occurring zeolites, in saline-alkaline lakes and cavities of mafic rocks, analcime has higher stability field at higher temperatures (100 degrees Celsius) (Figure 24) [13]. This is consistent with the models developed in this research; only the fly ash F geopolymer (with low CaO content) cured at 75 degrees Celsius contained analcime. Moreover, reduced aqueous silica activity favored the formation and stability of natrolite [13]. With increase in CaO content (addition of fly ash class C), analcime phase disappeared completely from the phase assemblage and was replaced by natrolite, $C-N-A-S-H$ (calcium sodium aluminosilicate hydrate) and $C-S-H$.

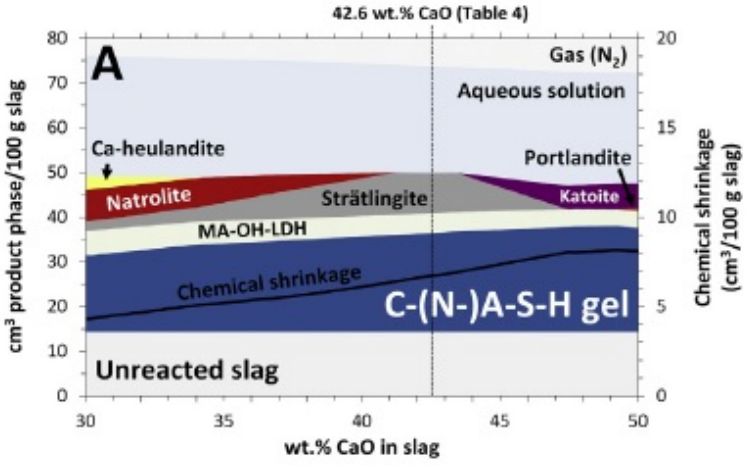

Figure 23: Simulated solid phase assemblage of alklali-activated slag at varying CaO content [66]

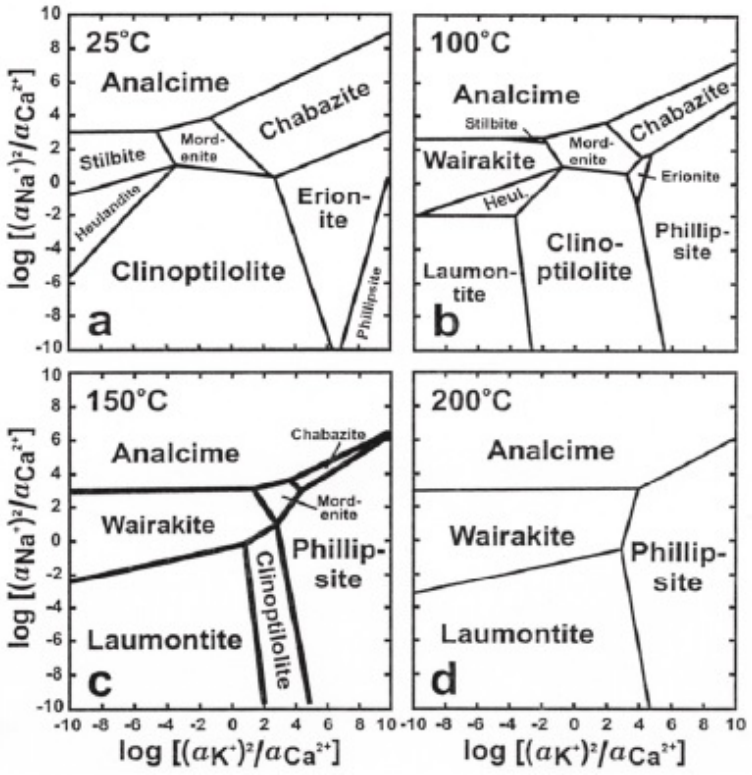

Figure 24: Zeolites occurring in hydrothermal deposits in silicic-volcanic rocks [13]

The formation of $C-N-A-S-H$ was observed in models of alkali-activated blast furnace slag developed by Myers et. al. [64, 66, 63]. In one of the studies [65], it was shown that the calcium sodium aluminosilicate hydrate can be highly cross-linked. Also, a cross-linked substituted tobermorite model was proposed (Figure 25). The addition of fly ash class C caused the formation of this phase in all F-C geopolymers in this study (section 4.2.3). This phase is resistant to the effects of hydrolytic attack [53] [75] and reduction in charge-balancing alkali cations (Na+ or K+).

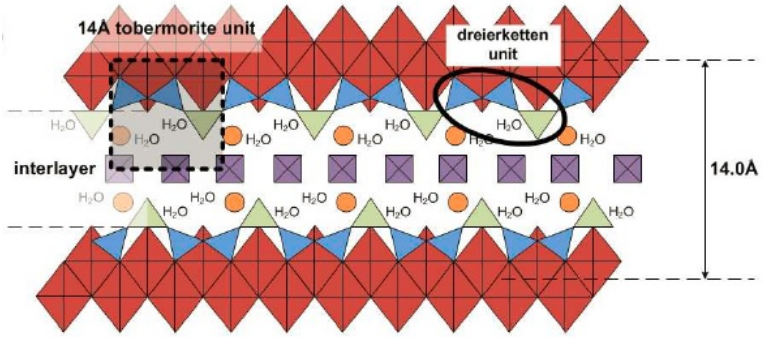

Figure 25: Cross-linked substituted tobermorite model. Red diamonds represent interlayer calcium and blue triangles represent paired tetrahedra [65]

In fly ash F geopolymer models developed in this study, with increase in wastewater content, the amount of zeolites decreased significantly. The percentages of total zeolites can be seen in different mixes at 10 and 30 percent wastewater content (table 23). The ion-rich FGD wastewater causes disintegration of zeolites by reacting with the charge-balancing alkali cations and sending the reversible reaction in favor of geopolymer molecule breakage. Based on the models developed, the following

Table 23: Water content with increase in FGD wastewater percentage

	Water Content (wt%)	
Mix Name	10 wt% FGD	30 wt% FGD
F-RT	31	16
F-OT	46	23
FC-RT	25	12
FC-OT	38	18

reactions can be triggered:

$$(Ca^{2+}, Na^{+}, K^{+}) - (-Si - O - Al^{-} - O - Si - O-) + 4nH_2O + Cl^{-} \rightarrow$$
$$n(OH)_3 - Si - O - Al^{-}(OH)_2 - O - Si - (OH)_3 + Nacl(halite), Ca(Cl)_2 or KCl \quad (37)$$

$$(Ca^{2+}, Na^{+}, K^{+}) - (-Si - O - Al^{-} - O - Si - O-) + 4nH_2O + SO_4^{2-} \rightarrow$$
$$n(OH)_3 - Si - O - Al^{-}(OH)_2 - O - Si - (OH)_3 + Na_2SO_4(Thenardite), Ca(SO_4)(gypsum),$$
$$K_2SO_4 \quad or \quad KAl_3(SO_4)_2(OH)_6 \quad (38)$$

The salts produced as a result of these reactions precipitate within the geopolymer matrix and causes discontinuity. Moreover, the soluble species like halite, thenardite and gypsum dissolve in aqueous environment and cause high leachability due to dissolution especially in case of sulfate (Section 4.1.1)

The other process that breaks the geopolymer molecule is hydrolytic attack [53] [75]. When the geopolymer molecules break (reactions 37 and 38), higher amount of water becomes available in the system. This trend is evident in models presented in the previous section (Chapter 4). Also, the additional water from FGD wastewater takes part in the hydrolytic attack as follows:

$$\equiv Si - O^{-}Na^{+} + HOH \rightarrow \equiv Si - OH + Na^{+} + OH^{-} \tag{39}$$

$$\equiv Si - O - Si \equiv + OH^{-} \rightarrow \quad \equiv Si - OH + \equiv Si - O^{-} \tag{40}$$

$$\equiv Si - O^{-} + HOH \rightarrow \quad \equiv Si - OH + OH^{-} \tag{41}$$

5.3 Future Research

The following topics would be new areas that can be explored in the future:

- Chemical characterization of alkali-activated fly ash contaminated by FGD wastewater would need more scrutiny. These types of studies have been performed on various alkali-activated materials using XRD and ^{27}Al and ^{29}Si MAS NMR (Magic-Angle Spinning Nuclear Magnetic Resonance Spectroscopy) and XRD (X-Ray Diffraction) techniques and deconvolution of the results [65]

- Exploring options for pretreatment of FGD wastewater before its sequestration in fly ash geopolymer. Treatment with solid sodium metasilicate would cause the wastewater precipitate and prevent it from precipitation in the geopolymer gel.

- Exploring ways for beneficiation of FGD wastewater including rare earth element extraction. This option is being used for coal fly ash [61, 27, 8, 33] and can be potentially used for FGD wastewater.

- Pursuing other options for developing a denser geopolymer matrix including the use of potassium silicate as the activator solution. As the charge-balancing ion K^+ is smaller in size, it provides a denser geopolymer tetrahedral structure [6, 40, 81].

- Using other aluminosilicate sources including blast furnace slag for the development of geopolymer.

REFERENCES

[1] E. Álvarez-Ayuso, X. Querol, and A. Tomás. Environmental impact of a coal combustion-desulphurisation plant: Abatement capacity of desulphurisation process and environmental characterisation of combustion by-products. *Chemosphere*, 65(11):2009–2017, 2006.

[2] J. W. Anthony, R. A. Bideaux, K. W. Bladh, and M. C. Nichols. Handbook of mineralogy, mineralogical society of america, chantilly, va 20151-1110, usa, 2011.

[3] G. Artioli, J. V. Smith, and Å. Kvick. Neutron diffraction study of natrolite, na2al2si3o10. 2h2o, at 20 k. *Acta Crystallographica Section C*, 40(10):1658–1662, 1984.

[4] A. C. A. Association et al. Coal combustion product production and use statistics, 2008.

[5] T. Bakharev. Geopolymeric materials prepared using class f fly ash and elevated temperature curing. *Cement and concrete research*, 35(6):1224–1232, 2005.

[6] V. F. Barbosa and K. J. MacKenzie. Synthesis and thermal behaviour of potassium sialate geopolymers. *Materials Letters*, 57(9-10):1477–1482, 2003.

[7] D. L. Bish and D. W. Ming. *Natural zeolites: occurrence, properties, applications*, volume 45. Walter de Gruyter GmbH & Co KG, 2019.

[8] R. Blissett, N. Smalley, and N. Rowson. An investigation into six coal fly ashes from the united kingdom and poland to evaluate rare earth element content. *Fuel*, 119:236–239, 2014.

[9] B. Cetin, A. H. Aydilek, and Y. Guney. Leaching of trace metals from high carbon fly ash stabilized highway base layers. *Resources, Conservation and Recycling*, 58:8–17, 2012.

[10] R. Charles. Static fatigue of glass. i. *Journal of Applied Physics*, 29(11):1549–1553, 1958.

[11] N. W. Chen-Tan, A. Van Riessen, C. V. Ly, and D. C. Southam. Determining the reactivity of a fly ash for production of geopolymer. *Journal of the American Ceramic Society*, 92(4):881–887, 2009.

[12] P. Chindaprasirt, T. Chareerat, S. Hatanaka, and T. Cao. High-strength geopolymer using fine high-calcium fly ash. *Journal of Materials in Civil Engineering*, 23(3):264–270, 2010.

[13] S. J. Chipera and J. A. Apps. Geochemical stability of natural zeolites. *Reviews in mineralogy and geochemistry*, 45(1):117–161, 2001.

[14] J. Davidovits. Geopolymer chemistry and applications. institut géopolymère (geopolymer institute): Saint-quentin, france, 2008. Technical report, ISBN 2-9514820-1-9.

[15] J. Davidovits. Geopolymer chemistry and properties. In *Geopolymer*, volume 88, pages 25–48, 1988.

[16] J. Davidovits. Geopolymers: inorganic polymeric new materials. *Journal of Thermal Analysis and calorimetry*, 37(8):1633–1656, 1991.

[17] J. Davidovits. Properties of geopolymer cements in first international conference on alkaline cements and concretes. *Scientific Research, Kiev, Ukraine*, 1994.

[18] J. Davidovits and G. Comrie. Archaeological long-term durability of hazardous-waste disposal-preliminary-results with geopolymer technologies. In *ABSTRACTS OF PAPERS OF THE AMERICAN CHEMICAL SOCIETY*, volume 195, pages 50–ENVR. AMER CHEMICAL SOC 1155 16TH ST, NW, WASHINGTON, DC 20036, 1988.

[19] B. Z. Dilnesa, B. Lothenbach, G. Renaudin, A. Wichser, and E. Wieland. Stability of monosulfate in the presence of iron. *Journal of the American Ceramic Society*, 95(10):3305–3316, 2012.

[20] K. Dombrowski, A. Buchwald, and M. Weil. The influence of calcium content on the structure and thermal performance of fly ash based geopolymers. *Journal of Materials Science*, 42(9):3033–3043, 2007.

[21] P. Duxson, A. Fernández-Jiménez, J. L. Provis, G. C. Lukey, A. Palomo, and J. Van Deventer. Geopolymer technology: the current state of the art. *Journal of Materials Science*, 42(9):2917–2933, 2007.

[22] U. EPA. Identification and listing of hazardous waste, toxicity characteristics. 40 cfr 261.24. *Federal Register*, 18(261):55–56, 1999.

[23] A. Fernández-Jiménez, A. Palomo, I. Sobrados, and J. Sanz. The role played by the reactive alumina content in the alkaline activation of fly ashes. *Microporous and Mesoporous materials*, 91(1):111–119, 2006.

[24] C. F. Ferraris. Measurement of the rheological properties of high performance concrete: state of the art report. *Journal of research of the national institute of standards and technology*, 104(5):461, 1999.

[25] G. Ferraris, D. Jones, and J. TERKESS. A neutron-diffraction study of the crystal structure of analcime, naalsi2o6· h2o. *Zeitschrift für Kristallographie-Crystalline Materials*, 135(1-6):240–483, 1972.

[26] B. A. Fillenwarth. Development of optimization models for the set behavior and compressive strength of sodium activated geopolymer pastes. 2013.

[27] W. Franus, M. M. Wiatros-Motyka, and M. Wdowin. Coal fly ash as a resource for rare earth elements. *Environmental Science and Pollution Research*, 22(12):9464–9474, 2015.

[28] R. W. Fuessle and M. A. Taylor. Long-term solidification/stabilization and toxicity characteristic leaching procedure for an electric arc furnace dust. *Journal of Environmental Engineering*, 130(5):492–498, 2004.

[29] M. G. Tajabadi. Unpublished work, 2015.

[30] Y. L. Galiano, C. F. Pereira, and J. Vale. Stabilization/solidification of a municipal solid waste incineration residue using fly ash-based geopolymers. *Journal of hazardous materials*, 185(1):373–381, 2011.

[31] E. M. Gartner and H. M. Jennings. Thermodynamics of calcium silicate hydrates and their solutions. *Journal of the American Ceramic Society*, 70(10):743–749, 1987.

[32] A. Gianoncelli, A. Zacco, R. P. Struis, L. Borgese, L. E. Depero, and E. Bontempi. Fly ash pollutants, treatment and recycling. In *Pollutant Diseases, Remediation and Recycling*, pages 103–213. Springer, 2013.

[33] V. Goldschmidt. Rare elements in coal ashes. *Industrial & Engineering Chemistry*, 27(9):1100–1102, 1935.

[34] G. Gottardi and E. Galli. *Natural zeolites*, volume 18. Springer Science & Business Media, 2012.

[35] M. L. Granizo, S. Alonso, M. T. Blanco-Varela, and A. Palomo. Alkaline activation of metakaolin: effect of calcium hydroxide in the products of reaction. *Journal of the American Ceramic Society*, 85(1):225–231, 2002.

[36] Q. Guo and E. J. Reardon. Calcined dolomite: alternative to lime for minimizing undesirable element leachability from fly ash. *Industrial & Engineering Chemistry Research*, 51(26):9106–9116, 2012.

[37] X. Guo, H. Shi, L. Chen, and W. A. Dick. Alkali-activated complex binders from class c fly ash and ca-containing admixtures. *Journal of hazardous materials*, 173(1):480–486, 2010.

[38] X. Guo, H. Shi, and W. A. Dick. Compressive strength and microstructural characteristics of class c fly ash geopolymer. *Cement and Concrete Composites*, 32(2):142–147, 2010.

[39] H. Haji-Esmaelii. *Admixtures for use in geopolymers*. PhD thesis, 2012.

[40] P. He, D. Jia, M. Wang, and Y. Zhou. Thermal evolution and crystallization kinetics of potassium-based geopolymer. *Ceramics International*, 37(1):59–63, 2011.

[41] H. C. Helgeson. Summary and critique of the thermodynamic properties of rock-forming minerals. *American Journal of Science*, 278:1–229, 1978.

[42] B. Henderson. For sale: Coal ash to right buyer, 2014.

[43] A. Irabien, I. F. Olmo, A. Andres, and M. Sebastia. Prediction of tclp leachates of electric arc furnace dust/cement products using neural network analysis. *Environmental Progress & Sustainable Energy*, 21(2):95–104, 2002.

[44] M. Izquierdo and X. Querol. Leaching behaviour of elements from coal combustion fly ash: an overview. *International Journal of Coal Geology*, 94:54–66, 2012.

[45] G. Johnson, H. Flotow, P. O'hare, and W. Wise. Thermodynamic studies of zeolites: analcime and dehydrated analcime. *Am. Mineral.;(United States)*, 67, 1982.

[46] G. Johnson, H. Flotow, P. O'Hare, and W. Wise. Thermodynamic studies of zeolites; natrolite, mesolite and scolecite. *American Mineralogist*, 68(11-12):1134–1145, 1983.

[47] I. K. Karpov, K. V. Chudnenko, and D. A. Kulik. Modeling chemical mass transfer in geochemical processes; thermodynamic relations, conditions of equilibria and numerical algorithms. *American Journal of Science*, 297(8):767–806, 1997.

[48] H. Kikkawa, T. Nakamoto, M. Morishita, and K. Yamada. New wet fgd process using granular limestone. *Industrial & engineering chemistry research*, 41(12):3028–3036, 2002.

[49] D. A. Kulik. Improving the structural consistency of csh solid solution thermodynamic models. *Cement and Concrete Research*, 41(5):477–495, 2011.

[50] D. A. Kulik, T. Wagner, S. V. Dmytrieva, G. Kosakowski, F. F. Hingerl, K. V. Chudnenko, and U. R. Berner. Gem-selektor geochemical modeling package: revised algorithm and gems3k numerical kernel for coupled simulation codes. *Computational Geosciences*, 17(1):1–24, 2013.

[51] S. Kumar, R. Kumar, and S. Mehrotra. Influence of granulated blast furnace slag on the reaction, structure and properties of fly ash based geopolymer. *Journal of Materials Science*, 45(3):607–615, 2010.

[52] W. Lee and J. Van Deventer. The effect of ionic contaminants on the early-age properties of alkali-activated fly ash-based cements. *Cement and Concrete Research*, 32(4):577–584, 2002.

[53] W. Lee and J. Van Deventer. The effects of inorganic salt contamination on the strength and durability of geopolymers. *Colloids and Surfaces A: Physicochemical and Engineering Aspects*, 211(2):115–126, 2002.

[54] W. Lee and J. Van Deventer. The interface between natural siliceous aggregates and geopolymers. *Cement and Concrete Research*, 34(2):195–206, 2004.

[55] W. Lee and J. J. van Deventer. Effects of anions on the formation of aluminosilicate gel in geopolymers. *Industrial & engineering chemistry research*, 41(18):4550–4558, 2002.

[56] C. Leiva, C. G. Arenas, L. Vilches, J. Vale, A. Gimenez, J. Ballesteros, and C. Fernández-Pereira. Use of fgd gypsum in fire resistant panels. *Waste Management*, 30(6):1123–1129, 2010.

[57] Z. Li and S. Liu. Influence of slag as additive on compressive strength of fly ash-based geopolymer. *Journal of Materials in civil engineering*, 19(6):470–474, 2007.

[58] B. Lothenbach, D. A. Kulik, T. Matschei, M. Balonis, L. Baquerizo, B. Dilnesa, G. D. Miron, and R. J. Myers. Cemdata18: A chemical thermodynamic database for hydrated portland cements and alkali-activated materials. *Cement and Concrete Research*, 115:472–506, 2019.

[59] B. Lothenbach and F. Winnefeld. Thermodynamic modelling of the hydration of portland cement. *Cement and Concrete Research*, 36(2):209–226, 2006.

[60] D. Macphee and I. Garcia-Lodeiro. Activation of aluminosilicates-some chemical considerations. In *Proceedings of Slag Valorisation Symposium*, pages 51–61, 2011.

[61] D. B. Mayfield and A. S. Lewis. Environmental review of coal ash as a resource for rare earth and strategic elements. In *Proceedings of the 2013 World of Coal Ash (WOCA) Conference, Lexington, KY, USA*, volume 2013, pages 22–25, 2013.

[62] Z. Miao, H. Yang, Y. Wu, H. Zhang, and X. Zhang. Experimental studies on decomposing properties of desulfurization gypsum in a thermogravimetric analyzer and multiatmosphere fluidized beds. *Industrial & Engineering Chemistry Research*, 51(15):5419–5423, 2012.

[63] R. J. Myers, S. A. Bernal, and J. L. Provis. A thermodynamic model for c-(n-) ash gel.

[64] R. J. Myers, S. A. Bernal, and J. L. Provis. A thermodynamic model for c-(n-) ash gel: Cnash_ss. derivation and validation. *Cement and Concrete Research*, 66:27–47, 2014.

[65] R. J. Myers, S. A. Bernal, R. San Nicolas, and J. L. Provis. Generalized structural description of calcium–sodium aluminosilicate hydrate gels: the cross-linked substituted tobermorite model. *Langmuir*, 29(17):5294–5306, 2013.

[66] R. J. Myers, B. Lothenbach, S. A. Bernal, and J. L. Provis. Thermodynamic modelling of alkali-activated slag cements. *Applied Geochemistry*, 61:233–247, 2015.

[67] D. Panias, I. P. Giannopoulou, and T. Perraki. Effect of synthesis parameters on the mechanical properties of fly ash-based geopolymers. *Colloids and Surfaces A: Physicochemical and Engineering Aspects*, 301(1):246–254, 2007.

[68] L. Pauling. The structure of some sodium and calcium aluminosilicates. *Proceedings of the National Academy of Sciences*, 16(7):453–459, 1930.

[69] C. F. Pereira, Y. Luna, X. Querol, D. Antenucci, and J. Vale. Waste stabilization/solidification of an electric arc furnace dust using fly ash-based geopolymers. *Fuel*, 88(7):1185–1193, 2009.

[70] C. F. Pereira, M. Rodrıguez-Piñero, and J. Vale. Solidification/stabilization of electric arc furnace dust using coal fly ash: analysis of the stabilization process. *Journal of hazardous materials*, 82(2):183–195, 2001.

[71] J. W. Phair, J. Van Deventer, and J. Smith. Mechanism of polysialation in the incorporation of zirconia into fly ash-based geopolymers. *Industrial & engineering chemistry research*, 39(8):2925–2934, 2000.

[72] J. L. Provis, G. C. Lukey, and J. S. van Deventer. Do geopolymers actually contain nanocrystalline zeolites? a reexamination of existing results. *Chemistry of materials*, 17(12):3075–3085, 2005.

[73] E. Shock. Slop98. dat (computer data file). *http://www. chnosz. net/download/slop98. edit. dat*, 1998.

[74] Sindhunata, J. Van Deventer, G. Lukey, and H. Xu. Effect of curing temperature and silicate concentration on fly-ash-based geopolymerization. *Industrial & Engineering Chemistry Research*, 45(10):3559–3568, 2006.

[75] M. Takata, M. Tomozawa, and E. Watson. Effect of water content on mechanical properties of na2o-sio2 glasses. *Journal of the American Ceramic Society*, 65(9), 1982.

[76] W. Taylor, C. Meek, and W. Jackson. The structures of the fibrous zeolites. *Zeitschrift für Kristallographie-Crystalline Materials*, 84(1-6):373–398, 1933.

[77] J. Van Jaarsveld, J. Van Deventer, and L. Lorenzen. The potential use of geopolymeric materials to immobilise toxic metals: Part i. theory and applications. *Minerals Engineering*, 10(7):659–669, 1997.

[78] J. Van Jaarsveld, J. Van Deventer, and A. Schwartzman. The potential use of geopolymeric materials to immobilise toxic metals: Part ii. material and leaching characteristics. *Minerals Engineering*, 12(1):75–91, 1999.

[79] C. E. White, J. L. Provis, T. Proffen, and J. S. van Deventer. Molecular mechanisms responsible for the structural changes occurring during geopolymerization: multiscale simulation. *AIChE Journal*, 58(7):2241–2253, 2012.

[80] W. B. White, S. M. Johnson, and G. B. Dantzig. Chemical equilibrium in complex mixtures. *The Journal of Chemical Physics*, 28(5):751–755, 1958.

[81] N. Xie, J. L. Bell, and W. M. Kriven. Fabrication of structural leucite glass–ceramics from potassium-based geopolymer precursors. *Journal of the American Ceramic Society*, 93(9):2644–2649, 2010.

[82] H. Xu and J. Van Deventer. The geopolymerisation of alumino-silicate minerals. *International Journal of Mineral Processing*, 59(3):247–266, 2000.

[83] J. Xu, Y. Zhou, Q. Chang, and H. Qu. Study on the factors of affecting the immobilization of heavy metals in fly ash-based geopolymers. *Materials letters*, 60(6):820–822, 2006.

[84] C. K. Yip, G. Lukey, and J. Van Deventer. The coexistence of geopolymeric gel and calcium silicate hydrate at the early stage of alkaline activation. *Cement and Concrete Research*, 35(9):1688–1697, 2005.

[85] L. Zheng, C. Wang, W. Wang, Y. Shi, and X. Gao. Immobilization of mswi fly ash through geopolymerization: effects of water-wash. *Waste Management*, 31(2):311–317, 2011.

[86] Y. Zuo, M. Nedeljkovic, K. Arbi, and G. Ye. Thermodynamic modeling and experimental study of alkali-activated slag paste'. In *Proceedings of 4th International Symposium on Ultra-High Performance Concrete and High Performance Construction Materials, Kassel*, pages 25–26, 2016.